

3D Printing of Multicomponent Hydrogels for Biomedical Applications

D. ZHOU,^{a,b,c,†} C. WANG,^{a,b,c,†} A. HERT,^{a,b,c} L. YAN,^{a,b,c} B. DOU^{a,b,c}
AND L. OUYANG^{*a,b,c}

^a Department of Mechanical Engineering, Tsinghua University, Beijing 100084, China; ^b Biomanufacturing and Engineering Living Systems Innovation International Talents Base (111 Base), Tsinghua University, Beijing 100084, China; ^c Biomanufacturing and Rapid Forming Technology Key Laboratory of Beijing, Tsinghua University, Beijing 100084, China
*Email: ouy@tsinghua.edu.cn

8.1 Introduction

Hydrogels have attracted much attention in biomedical applications owing to their unique properties such as high-water content, good biocompatibility, mechanical flexibility, and structural relevance to biological tissues.^{1,2} The advances in polymer chemistry and a better understanding of material–cell and material–tissue interactions have allowed researchers to modify hydrogel properties to better fit into various biomedical application scenarios. An essential strategy is to develop multicomponent hydrogel formulations and structures to share the desirable features obtained from individual components.¹ This strategy might address some critical issues of

[†]These authors contributed to the work equally.

single-component hydrogels, such as the difficulty of recapitulating the heterogeneous structures of biomedical devices² and functionally engineered tissues.^{3,4} Despite the progress in new chemistry and materials preparation, the processing of generally soft and fragile hydrogels into desired structures remains an enduring challenge.² Therefore, a flexible manufacturing technique is needed to satisfy various application demands. 3D printing, also known as additive manufacturing, is a desirable technology for integrating hydrogel materials to construct customized multicomponent structures following the digital model guidance through computer-aided design/computer-aided manufacturing. It has specific advantages such as free-form and heterogeneous fabrication compared to traditional subtractive manufacturing approaches. For these reasons, hydrogel-based materials combined with 3D printing are becoming increasingly important.

Notably, no single technique can achieve the 3D printing of all kinds of hydrogels, and no single type of hydrogel can satisfy all application requirements. Various enabling techniques of 3D printing have been used to process hydrogels, including extrusion-, jet- and vat polymerization-based approaches, which all have their advantages and disadvantages. Various forms of multicomponent hydrogel ink for 3D printing have also been developed, including miscible multi-material or multi-network and immiscible composite hydrogels.² Considering the rapid progress in the field, we believe a thorough understanding of 3D printing techniques and the requirements for hydrogels in 3D printing is beneficial to efficiently determine the printing strategy for particular biomedical applications. This chapter will introduce the basic principles of hydrogel printing techniques, the strategies for formulating multicomponent hydrogel inks for 3D printing, and the most recent advances in typical biomedical applications. It aims to help the readers better understand the principles and state-of-the-art 3D printing of multicomponent hydrogels and inspire them when developing hydrogels and 3D printing techniques for biomedical use.

8.2 3D Printing Technologies

3D printing was initially developed to rapidly manufacture a prototype without additional cutting or casting methods. In 1981, Hideo Kodama developed a rapid prototyping system in Japan based on an ultraviolet (UV) polymerization manner. It presents a new way of fabricating a solid model by stacking the cross-sectional layers *via* curing the liquid photo-hardening polymer quickly without excessive manual labor.⁵ Chuck Hull invented stereolithography (SLA) technology, filed the world's first patent in 3D printing in 1984, and started commercialization in 1987.³ Since then, 3D printing has been seen with considerable progress in the enabling techniques and applicable materials. 3D printing of hydrogels has attracted much attention considering the difficulty of processing hydrogels using conventional manufacturing approaches. Here we will review the hydrogel 3D printing technologies and categorize them into three types, namely, extrusion-, jet- and vat polymerization-based 3D printing (see Table 8.1).

Table 8.1 Characteristics of various 3D printing technologies.⁶⁻²⁰

Category	Technology	Main feature(s)	Resolution	Viscosity of inks
Extrusion-based	Multiple-channel integrated extrusion	<ul style="list-style-type: none"> • Enable continuous multi-material extrusion <i>via</i> integration of multichannels into one outlet or multiple outlets 	> 80 μm	$30-6 \times 10^7$ mPa s
	Template extrusion	<ul style="list-style-type: none"> • The scale and shape of the core-shell structure can be tuned by the coaxial nozzle and pre-set cartridge 	> 10 μm (determined by the nozzle diameter and its inside structure)	
	Freeform-support extrusion	<ul style="list-style-type: none"> • Enable omnidirectional printing within the non-miscible supporting medium • Optional crosslinking strategy to remove the supporting medium or printed materials to obtain positive or negative structure 	> 20 μm	Can be widely varied depending on the crosslinking mechanisms and supporting bath properties
Jet-based	Inkjet printing	<ul style="list-style-type: none"> • Vaporizable materials are required in thermal inkjet printing 	> 50 μm	3.5-30 mPa s
	Micro-valve printing	<ul style="list-style-type: none"> • Droplet size depends on the diameter of the orifice • Enable drop-on-demand printing and continuous filament printing by controlling the valve opening time 	~ 150 μm	1-70 mPa s

Table 8.1 (Continued)

Category	Technology	Main feature(s)	Resolution	Viscosity of inks
		<ul style="list-style-type: none"> • Enable simultaneously or sequentially printing multiple materials with individual manipulation of multi-valves 		
	Electrohydrodynamic jet printing	<ul style="list-style-type: none"> • Droplets can be smaller than orifice • Enable to produce both directed and unordered structures with nanofibers • Mild pressure to eject the materials due to the pulling under the electric field 	> 50 nm	> 2000 mPa s
	Laser-induced forward printing	<ul style="list-style-type: none"> • The introduction of the absorbing layer avoids shear stress and direct thermal effect on the ink 	10–100 μm	1–300 mPa s
	Acoustic printing	<ul style="list-style-type: none"> • Enable both orifice-free and orifice printing 	5–300 μm	< 18 mPa s
	Aerosol jet printing	<ul style="list-style-type: none"> • A primary process of aerosol generation <i>via</i> pneumatic or ultrasonic atomizer is indispensable • The sheath gas enables direct aerosol writing with high resolution • Enable printing porous structures without the sacrifice-supporting structure 	> 85 nm	0.7–2500 mPa s

Vat photopolymerization-based	Stereolithography	<ul style="list-style-type: none"> • A single light beam directly induces the resin polymerization • Dynamic mask directly projects the 2D light slice to cure the resin under the control of a digital micromirror device • An oxygen-permeable film is introduced to establish the “dead zone” to support continuous photopolymerization processes • Smooth objects without slicing trace • A small spatial spot (voxel), caused by the simultaneous absorption of three or more photons, is applied to cure the resin • Enable omnidirectional polymerization within the transparent vat • Enable rapid polymerization without the sacrifice-supporting structure inside the transparent vat • Smooth surface of the printed object without anisotropies 	> 0.6 μm	No limitation unless the resin replenishing process is suppressed; low viscosity benefits the printing resolution
	Digital light processing		> 25 μm	
	Continuous liquid interface production		50 μm	Fluidity of resin should be maintained to achieve the continuous printing
	Multiphoton polymerization		> 80 nm	High viscosity resin without fluidity limitation
	Volumetric 3D printing		80 μm positive and 500 μm negative (computed axial lithography) 25 μm (xolography)	High viscosity resin and even the solid resin are possible

8.2.1 Filament Extrusion-based 3D Printing

Extrusion-based 3D printing is the most commonly used technique for hydrogel printing due to its easy availability and high capability for printing complex structures.² Driven by pneumatic, mechanical, screw, or electrical forces, hydrogel precursor solutions are extruded through a narrow nozzle to form filament-shaped building blocks, usually deposited on a receiving substrate layer by layer in a computer-controlled fashion. Different strategies can be adopted for the 3D printing of multicomponent hydrogels as follows (Figure 8.1).

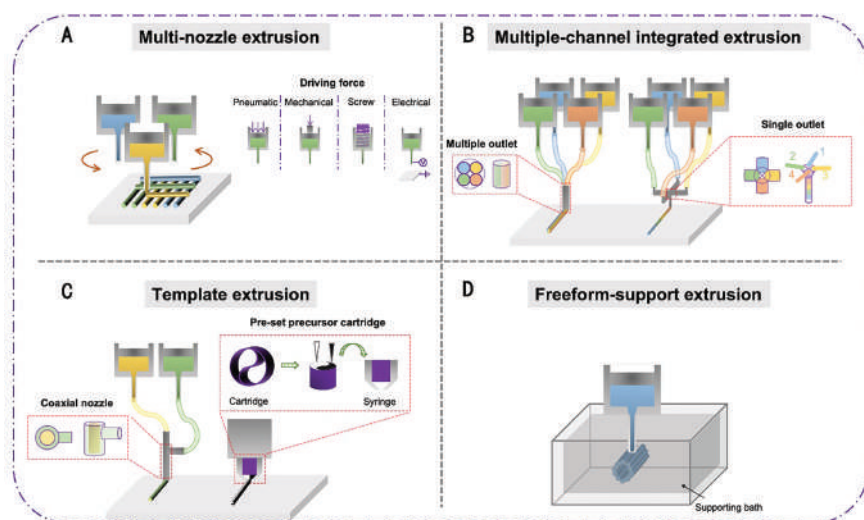


Figure 8.1 Schematics of filament extrusion-based 3D printing technologies. (A) Multi-nozzle extrusion. Syringes loaded with different materials automatically shift to print a multi-component structure following the pre-design program. (B) Multiple-channel integrated extrusion. In the multiple outlet approach, outlets of various materials are assembled so that hydrogels can be extruded as an anisotropic hydrogel filament simultaneously or orderly. In the single outlet approach, channels of various materials are integrated into one outlet *via* manipulative valves, which sequence hydrogels to form the anisotropic or heterogeneous filament. (C) Template extrusion. In the coaxial nozzle, core and shell hydrogel solutions, respectively, flow into the two (or more) entrances of the coaxial nozzle and contact in the confluence to form the core-shell filament. In the pre-shape cartridge, multiple hydrogel precursor solutions are loaded in corresponding areas inside the syringe. The precursor makes adaptive flow (under air or hydraulic pressure) to the nozzle to generate the scaled-down filament with the pre-shape pattern. (D) Freeform-support extrusion. The filament can be printed and immobilized in any direction within the bath to form an overhanging object regardless of the layer-by-layer manner.

8.2.1.1 Multiple-nozzle Extrusion

Printing with multiple nozzles loaded with different inks is a straightforward way to fabricate multi-component hydrogels. Sun *et al.* patented their multiple-nozzle extrusion-based 3D printing technology in 2005, which was initially designed to fabricate heterogeneous cell-laden hydrogel constructs.⁴ Similarly, Kang *et al.* developed an integrated tissue–organ printer (ITOP) to achieve the printing of ear cartilage with multi-materials (polycaprolactone (PCL), Pluronic F-127, and cell-laden composite hydrogels), and the printed implantable structure (see Figure 8.2A) exhibited desirable potential in promoting ear cartilage reconstruction.²¹ Multiple-nozzle 3D printers are currently available from numerous 3D printing companies and have been widely used in processing hydrogel-based products. Each ink material is loaded in a separate nozzle unit and deposited independently (see Figure 8.1A). While the interfaces between different inks are usually sharp, the spatial resolution of heterogeneity is highly limited by the single nozzle printing resolution. In addition, the frequent transition of multiple nozzles during printing might compromise the printing speed and the repositioning deviation.

8.2.1.2 Multiple-channel Integrated Extrusion

Integrating multiple channels into a single deposition nozzle could physically avoid the transition and reposition of different nozzles. Instead, the switching of different inks is achieved by switching the individual channels before reaching the nozzle outlet, which could save printing time and achieve higher resolution (see Figure 8.1B). Using this approach, Liu *et al.* successfully printed up to seven hydrogel formulations to pattern organ-shaped heterogeneous structures, such as the brain, lungs, and heart (see Figure 8.2B).²² In their setup, the ending tubular outlet of multiple channels is packed together to form a multiple-channel outlet, which can easily generate parallel and tight filament with multiple materials.^{22,27} However, the packing of channel outlets would enlarge the diameter of the ending nozzle and thus might compromise the printing resolution and result in off-center filaments when only switching on the outer outlets during printing. Converging the channels into one outlet can avoid the problem. Lewis *et al.* developed a module printer based on the channel converging technique. The assembly of multiple module-printer allows for synchronizing printing of symmetrical structures with multiple nozzles, which considerably shortens the fabrication process (see Figure 8.2C).²³

8.2.1.3 Template Extrusion

The shape of filament can be altered by the nozzle shape during the extrusion process, which leads to the template extrusion printing of multi-component hydrogels (see Figure 8.1C). Coaxial nozzle printing is a typical

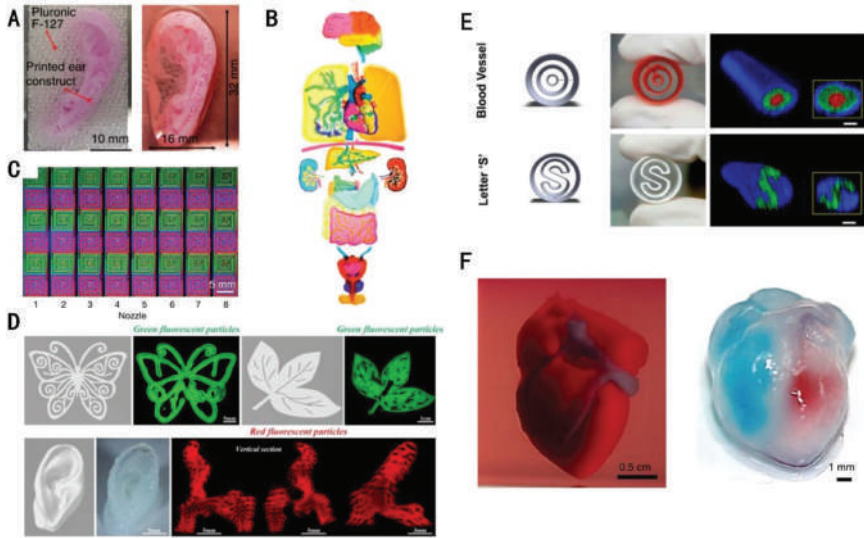


Figure 8.2 Representative examples of extrusion-based 3D printing. (A) The ear cartilage constructs were printed with a cell-laden hydrogel and sacrificial Pluronic F-127 (left) was dissolved in a cold medium (right). Adapted from ref. 21 with permission from Springer Nature, Copyright 2016. (B) The organ-like patterns were independently constructed with multiple bioinks in the multiple-channel integrated extrusion method and stitched together in the same image as the counterpart of the human body. Adapted from ref. 22 with permission from John Wiley & Sons, Copyright © 2016 Wiley-VCH Verlag GmbH & Co. KGaA, Weinheim. (C) The spiral patterns with four color silicone were printed by a four-material multiple-module printer. Adapted from ref. 23 with permission from Springer Nature, Copyright 2019. (D) Coaxial nozzle bioprinting structure with hollow filament, 2D butterfly and leaf patterns (top) and a solid ear model (bottom). Adapted from ref. 24 with permission from IOP Publishing, Copyright 2020. (E) Pre-set extrusion templates and the printed counterpart structures. Adapted from ref. 25, <https://iopscience.iop.org/article/10.1088/1758-5090/aac70b>, under the terms of the CC BY 3.0 license, <https://creativecommons.org/licenses/by/3.0/>. (F) The centimeter-sized heart is printed within a support bath (left). After extraction, red and blue dyes were injected into the left and right ventricles, respectively (right). Adapted from ref. 26, <https://doi.org/10.1002/advs.201900344>, under the terms of the CC BY 4.0 license, <https://creativecommons.org/licenses/by/4.0/>.

strategy of template printing to generate a continuous multi-layered coaxial filament with either solid or hollow cores,²⁸ the latter of which could be used for perfusion. Besides tubular tissue constructs, the coaxial printing approach has also been used to print hollow filaments to form complex structures with hollow channels (see Figure 8.2D).²⁴ Additionally, the coaxial nozzle can be combined with jet-based printing techniques to produce core-shell spheroids²⁹ or core-shell nanofibers.³⁰ In other examples, researchers have developed customized templates. Kang *et al.* prepared a home-made

pre-set precursor cartridge to locate and template cell-laden collagen and alginate hydrogels (see Figure 8.2E).²⁵ In this technique, inks are preloaded in the desired position of the precursor cartridge, then the precursor cartridge is inserted within a typical syringe reservoir. A hydrogel filament with a pre-set structure in the cross-section could be generated under the back-pressure. This methodology could theoretically obtain precise and customized heterogeneous filament building blocks. Still, it might meet the practical difficulty of preloading multi-materials and achieving simultaneous extrusion of these materials, especially when they exhibit distinct rheological properties.

8.2.1.4 Freeform-support Extrusion

In a typical extrusion-based hydrogel printing process, the ink usually passes through the nozzle in a liquid or semi-gel state and gels under external or internal stimuli on the substrate to self-support and support the upper layers for prevention from collapsing.³¹ A successful printing highly relies on the rapid gelation property of the hydrogels to maintain the structural fidelity and provides support for further printing. Instead of printing on a receiving substrate in the air, researchers have developed a free-support extrusion strategy based on a dual-layer reservoir in which the lower layer (gel or semi-gel state) immobilizes the extruded ink, and the upper layer (liquid state) replenishes the void space caused by the nozzle moving.³² Further, the emergence of the integrative supporting medium³³ liberates the requirement of the additional liquid layer and brings several advantages, such as more stable supporting, a shorter fabrication process, and higher printing resolution. In the printing process, the ink materials are extruded directly into a supporting bath composite of specific medium formulations with significant shear-thinning properties. During printing, the solid (or semi-gel) medium around the moving nozzle makes a quick transition to fluid states (shear-thinning), allowing the nozzle to deposit the ink (see Figure 8.1D). Simultaneously, a spontaneous recovery (self-healing) turns the medium back to a solid (or semi-gel) state, providing an encapsulation environment to support the deposited inks. The final printed structure can be collected after removing the supporting medium. Compared to the typical layer-by-layer printing in the air, this freeform-support extrusion technique allows the nozzle to print in any direction within the bath. Additionally, this approach allows for the fabrication of large-scale structures since the supporting medium can minimize the evaporation and possibly provide nutrition for printed cells during a lengthy printing process. However, the available materials are restricted by the properties (*e.g.*, transition temperature, load-bearing capacity) of the supporting medium.³⁴ With this technique, researchers printed various hydrogel-based models with complex structures (see Figure 8.2F), such as the continuous hierarchically branched tubular networks,³³ the tri-leaflet heart valve,⁷ and the dual cell-laden heart model.²⁶

8.2.2 Droplet Jet-based 3D Printing

Droplet jet-based 3D printing includes continuous and drop-on-demand approaches. In the early inkjet printing approach, droplets continuously pass through an electrostatic field for charging. Subsequently, the charged droplets are deflected to a substrate by a deflection field for patterning, while the uncharged droplets are directed to a gutter for recycling.³⁵ The low printing resolution and potential contamination during the recycling process have made the continuous inkjet approach less applicable in biomedical applications. The drop-on-demand methods can potentially address these issues and have mostly represented the so-called droplet jet-based printing. Droplet jet-based printing, widely applied in 2D patterning, generates droplets and deposits them on the substrate in a computer-controlled manner. This technology can also be used to deposit materials on the irregular surface due to its non-contact and self-adaptive properties. Additionally, a three-dimensional mobile platform enables 3D object printing. Here we summarize the droplet jet-based printing approaches as follows (see Figure 8.3) according to the mechanisms of droplet generation.

8.2.2.1 Inkjet Printing

Thermal and piezoelectric inkjet printing technologies are the most common drop-on-demand approaches. In thermal inkjet printing, the resistive element inside the thermal printer could rapidly heat up to almost 300 °C within a few microseconds to evaporate an air bubble and thus eject the droplet through the orifice (see Figure 8.3A). Subsequently, the ink fills back the chamber and gets ready for the next ejection. Although the heating process only lasts for a few microseconds, the hydrogel and encapsulated cargos with rigorous thermosensitivity may be functionality damaged. Additionally, hydrogels with high viscosity or non-vaporization properties are not suitable for thermal printing. Piezoelectric printing is an alternative approach, which ejects the droplet under the driving force from a sudden variation within the fluid chamber by applying a voltage pulse to the incorporated piezoceramics (see Figure 8.3A), and it expands the window of applicable inks because it frees the requirement for vaporizable materials.

Due to the high throughput and stable printing process, inkjet printing has been widely applied in generating a microarray of various biological materials, including DNA, proteins, and cells.⁴³ The multiple-nozzle strategy could also be incorporated with inkjet printing for printing multi-materials in microarray printing⁴⁴ and surface coating.⁴⁵ For example, three kinds of cell-laden inks were deposited to form the Eiffel tower pattern using this strategy (see Figure 8.4A).³⁶ Additionally, accompanied by the Z-axis direction movement, the multiple-nozzle strategy can print a 3D tubular cell-laden hydrogel structure (see Figure 8.4B).³⁷

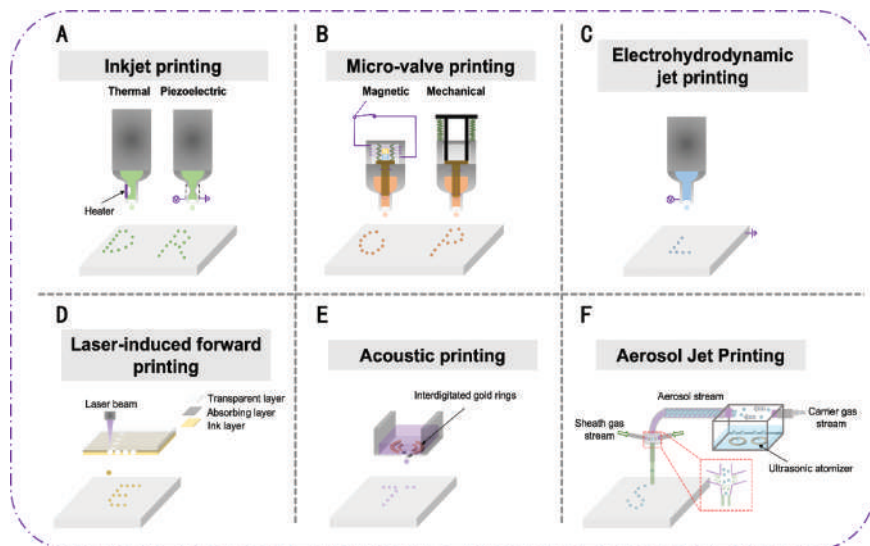


Figure 8.3 Schematics of droplet jet-based 3D printing technologies. (A) Inkjet printing. In the thermal printer, a heater is a crucial component to translate the electrical signal into a heat signal for evaporating the localized ink to eject. In the piezoelectric printer, piezoceramics distort spontaneously under the electric pulse leading to the variation of the chamber to achieve droplet ejection. (B) Micro-valve printing generates the droplets by altering the open–close state of the outlet *via* the magnetic or mechanical valve. (C) Electrohydrodynamic jet printing. The tunable DC electric field applied between the outlet (positive) and the substrate (negative) provides force to pull out droplets. (D) Laser-induced forward printing. The transparent layer allows the movable laser beam to focus on the absorbing layer, which can absorb the heat to induce an air bubble to eject droplets out of the ink layer. (E) Acoustic printing. The interdigitated gold rings produce circular waves and form an acoustic focal point at the interface between the air and the bioink to eject droplets. (F) Aerosol jet printing. The ink forms droplets under the mechanical vibrations caused by the ultrasonic atomizer. The carrier gas stream transports the droplets from the cartridge to the outlet, which is encircled by the sheath gas.

8.2.2.2 Micro-valve Printing

Micro-valve printing relies on a valve to switch the on/off state of the outlet, which allows the ink to be cut and ejected as droplets. The valve usually comprises a magnetic or mechanical actuator connecting to a plunger and springs (see Figure 8.3B). For the former, the voltage pulse is applied to induce a magnetic field in the solenoid coil to pull the plunger upwards.⁴⁶ Simultaneously, the ink passes through and then the plunger returns to block the ink as springs restore when the magnetic field disappears. For the mechanical valve-based approach, the vertical force is directly applied to the plunger to close the outlet. When the force is absent, the restoration of

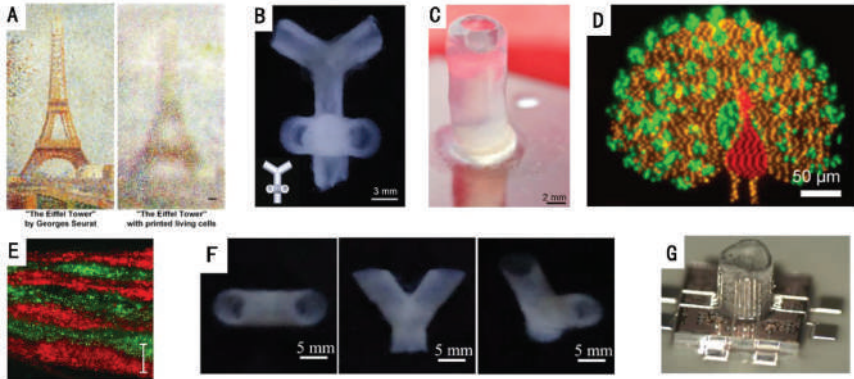


Figure 8.4 Representative examples of jet-based 3D printing. (A) The Eiffel tower by Georges Seurat pattern was printed with three types of cells labelled with different colours. Adapted from ref. 36, <https://doi.org/10.1038/s41598-017-14726-w>, under the terms of the CC BY 4.0 license, <https://creativecommons.org/licenses/by/4.0/>. (B) A bifurcation structure with both horizontal and vertical hollow features was printed with cell-alginate ink. Adapted from ref. 37 with permission from John Wiley & Sons, Copyright © 2014 Wiley Periodicals, Inc. (C) A 13 mm alginate tube structure was printed by dual-nozzle printing. Adapted from ref. 38, <https://iopscience.iop.org/article/10.1088/1758-5090/7/4/044102>, under the terms of the CC BY 3.0 license, <https://creativecommons.org/licenses/by/3.0/>. (D) A printed peacock image comprising three fluorescently labelled proteins. Adapted from ref. 39 with permission from American Chemical Society, Copyright 2012. (E) A seven-layer structure constructed by alternately printing red and green keratinocyte sublayers. Adapted from ref. 40 with permission from John Wiley & Sons, Copyright © 2012 Wiley Periodicals, Inc. (F) Images of Y-shaped alginate tubes printed. Adapted from ref. 41 with permission from IOP Publishing, Copyright 2015. (G) The vertical metal lines onto the wall of the dielectric pillar printed by aerosol jet printing (AJP). Adapted from ref. 42 with permission from IOP Publishing, Copyright 2015.

springs results in the opening of the outlet where the ink can pass through. Therefore, the throughput rate of ejection can be manipulated by tuning the electric pulse (magnetic) or force frequency (mechanical). Due to the individual manipulation of the valve, micro-valve printing supports the printing of multiple materials simultaneously or sequentially in an integrated multiple-nozzle system. Shu's group managed to produce spheroids of embryonic stem cells with various cell concentrations *via* a deliberate design, in which one nozzle decreasingly delivers the cell ink, while the other nozzle increasingly delivers the medium for maintaining the constant volume of each spheroid.⁴⁷ Further, they applied the dual nozzle approach to fabricate a 3D tubular structure by the ejection of alginate and calcium in an alternate manner (see Figure 8.4C).³⁸ Compared to inkjet printing, micro-valve printing possesses a higher driving force for ejection and can be applied to materials with higher viscosity. However, to minimize the damage of

shear stress on cells, the orifice diameter is supposed to be larger than the resulting droplet diameter.⁴⁸

8.2.2.3 Electrohydrodynamic Jet Printing

Electrohydrodynamic jet printing (EJP) is a high-resolution printing technology where the ink can be pulled out as a droplet or continuous fiber under an electric field (see Figure 8.3C). Initially, the ink in the cartridge is pushed to the nozzle driven by the backpressure, while the surface tension at the nozzle tip limits the ink from falling. Then an eclectic voltage is applied between the nozzle (usually metal-coated) and the substrate receiver. Simultaneously, the liquid ink is elongated to form the meniscus surface at the outlet and can further eject in the dripping mode (droplet generation) or jet mode (continuous fiber generation) by tuning the parameters.⁴⁹ The ejection process of EJP relies on multiple factors such as the properties of ink (viscosity and conductivity), electric voltage, nozzle diameter, and the distance between the nozzle and the substrate.^{49,50} In the dripping mode, the liquid meniscus gets elongated due to the combined effects of gravity force (liquid volume) and the electric force (electric voltage), which make the droplet detach from the tail of the elongated meniscus. Two stable stages of droplets, the gravity-leading large drops (\geq nozzle diameter) and the electric-leading small drops ($<$ nozzle diameter), can be generated, respectively, by tuning the ratio of the ink flow rate and electric voltage.⁵⁰ For the jetting mode, the formation of the Taylor cone represents the transition of EJP from the dripping mode to jet mode, where the liquid meniscus deforms into a conical shape.⁴⁹ This jetting mode has been adapted in the electrospinning and electrohydrodynamic-direct-writing (electrowriting) technologies. Additionally, the multiple materials printing strategy in extrusion-based printing is also applicable to EJP. Shigeta *et al.* succeeded in printing a peacock pattern (~ 300 μm) with three kinds of fluorescent proteins using a multi-nozzle printer (see Figure 8.4D).³⁹ Li's group applied the coaxial nozzle in EJP to achieve the cell-laden alginate direct printing core (collagen)–shell (alginate) multi-hydrogel cellular structure.⁵¹ Additionally, this strategy can be extended to the core–shell droplet generation.

8.2.2.4 Laser-induced Forward Transfer

Laser-induced forward transfer (LIFT), an orifice-free printing technology with high resolution, ejects ink droplets *via* vapor caused by a laser spot (see Figure 8.3D). This printing system normally consists of a pulsed laser beam for positioning, a donor ribbon for ejection, and a substrate for collection. As a start, the laser beam executes the printing motion to the pre-set position. Then the laser spot focuses on the ribbon comprising a transparent layer (*e.g.*, glass), an absorbing layer (*e.g.*, titanium), and an ink layer. The focal area of the absorbing layer produces a vapor bubble pushing the ink forward, and the resulting droplet lands on the facing substrate coated with a

hydrogel or other materials (protecting the droplet from vaporization). Importantly, to achieve successful ejection, the energy density of the applied laser beam should reach the threshold of vaporizing the absorbing materials. The laser energy can also affect the droplet size and geometry; the increase of focal area usually results in a larger droplet, while the excessive energy might cause the formation of irregular droplets or satellite droplets.⁵² It should be noted that the introduction of materials from the absorbing layer is nearly negligible because the absorbing layer is far thinner than the ink layer.⁵³ Besides, the metal materials stuck to the substrate can be easily washed away.⁵³ However, the encapsulation of the metal micro/nanoparticles within the hydrogel droplets is unavoidable, and its amount in droplets grows as the laser energy increases, so precise control of the exposure process during printing is essential to ease the contamination.⁵⁴ It is flexible to directly generate cell-laden hydrogel droplets by depositing the alginate onto the substrate coated with a calcium-containing gelatin hydrogel.⁵⁵ For printing multiple hydrogel materials, strategies of multi-ribbons⁵⁶ or one ribbon with multi-materials (side by side)⁴⁰ were both investigated to print the alternating pattern. Koch *et al.* fabricated a 3D grid structure by alternately printing dual materials (alginate with different cells) (see Figure 8.4E).⁴⁰ However, due to the poor mechanical properties, the structure of the liquid-state hydrogel droplets deforms as the printing layers accumulate, which leads to the low fidelity of the final structure. Localized crosslinking of the structure can improve the mechanical properties of the structure by transitioning the liquid-state hydrogel to a semi-gel/gel state, contributing to the support for the next layer deposition.⁵⁷ With modification, Xiong *et al.* managed to deposit alginate on the platform submerged in calcium solution to achieve Y-shaped tubular structure fabrication with LIFT (see Figure 8.4F).⁴¹ However, it is challenging to deposit multiple materials with different crosslinking mechanisms in this strategy.

8.2.2.5 Acoustic Printing

Acoustic printing generates a droplet *via* the application of the surface acoustic wave (see Figure 8.3E). The key functional part is a surface acoustic wave generator based on a piezoelectric substrate coated with interdigitated gold rings that determine the resonant frequency and wavelength of surface acoustic waves.¹⁰ When the printing begins, surface acoustic waves diffract into the liquid, and the symmetrical wave with circular geometry forms an acoustic focal plane resulting in disturbances at the air-liquid surface. When the acoustic radiation force exceeds the surface tension, the bulge liquid forms an elongated jet, and the abruptness at the end of the jet generates a droplet that lands on the collecting substrate. Acoustic printing is applicable for cell printing. For example, Demirci *et al.* successfully printed single cell-laden agarose hydrogel droplets ($\sim 37 \mu\text{m}$).⁵⁸ Additionally, the hydrogel solution with high cell density is also suitable for acoustic printing. Gong *et al.* exploited an acoustic printing system to eject a controllable droplet of

Matrigel with high cell density (3×10^7 cells per ml) to generate tumor organoids with a desirable repeatability.⁵⁹ The stability of the acoustic waves is noteworthy during the printing process. To avoid the liquid surface vibration caused by the movement, the mobile platform assembled to the collecting substrate has been used.⁶⁰ Acoustic printing can also be adopted in multi-material printing. Fang *et al.* placed a plate with wells on the water surface and aligned the surface of the materials in wells with the focal point of the transducer to eject the droplets so that a multi-component droplet array could be generated by focusing the acoustic wave on different wells.⁶¹ The acoustic wave propagation phenomenon within the medium can be applied to directly assemble particles (even a single cell) in a spatial direction without physical contact.⁶² Therefore, an acoustic field was set under the droplet generator to manipulate the passing droplets to form a pattern on the collecting substrate.⁶³ Acoustic force can also be applied as the driving force to improve the printability of droplet-based printing. Foresti *et al.* established an acoustic field around the outlet of the nozzle to generate acoustic force, which can achieve ejection of materials with a wide viscosity range (0.5–25 000 mPa s).⁶⁴

8.2.2.6 Aerosol Jet Printing

AJP exhibits non-contact and direct-write characteristics and can perform high-resolution printing.⁶⁵ The ink in the aerosol chamber first gets atomized by a pneumatic or ultrasonic atomizer as a dense aerosol, and subsequently the inert air-fluid (a carrier) transports these aerosols to a vertical channel, which guides the aerosols towards a movable substrate to print the desired features (see Figure 8.3F). To prevent the spread of the aerosols, an annular tube is usually set centered outside the nozzle, and the sheath gas from the tube synchronously jets to focus the aerosols between the nozzle and substrate.¹² Within the deposition head, the droplet diameter of the aerosol is 1–5 μm , and the aerosol stream impacts the substrate at a velocity of 10–100 m s^{-1} with the acceleration of the sheath gas.⁶⁵ The AJP technique has been used in manufacturing electronic components for biomedical applications such as biosensors⁶⁶ and flexible/wearable bio-electronic devices.⁶⁷ The AJP process is highly dependent on the rheological properties of the ink⁶⁸ and shows desirable performance in printing materials containing nano/microparticles of polymers⁶⁹ or metals.⁷⁰ Printability of UV curable materials was also proven in AJP. Rahman *et al.* printed acrylic urethane solution (containing silver nanoparticles) by cooperating with a UV ray for *in situ* curing to fabricate a dielectric pillar (see Figure 8.4G).⁴² Besides, AJP allowed high-resolution printing of the complex hierarchical porous structures (five orders of magnitude in the length scale) without support.⁷⁰ Similar to the multi-nozzle strategy, Tait *et al.* patterned parallel alignments of emitting organic light-emitting diodes *via* depositing three kinds of materials in sequence.⁷¹ It is noted that the possible dehydration phenomenon of hydrogel materials contributed by airflow during printing should be considered.

8.2.3 Vat Photopolymerization-based 3D Printing

Vat photopolymerization-based 3D printing is the general term for lithography-based printing technologies which directly exploit light to trigger or guide the polymerization of photosensitive materials to form a pre-designed structure, where a vat of photo-resins is selectively cured by light-activated polymerization (see Figure 8.5). Different from extrusion-based and droplet jet-based 3D printing, the ink materials and the printed structure are in contact during the printing process in vat photopolymerization-based printing. Therefore, manipulating the accumulated exposure dose such as grayscale light⁷² and exposure time⁷³ can tune the curing process for heterogeneous structure fabrication. However, vat photopolymerization

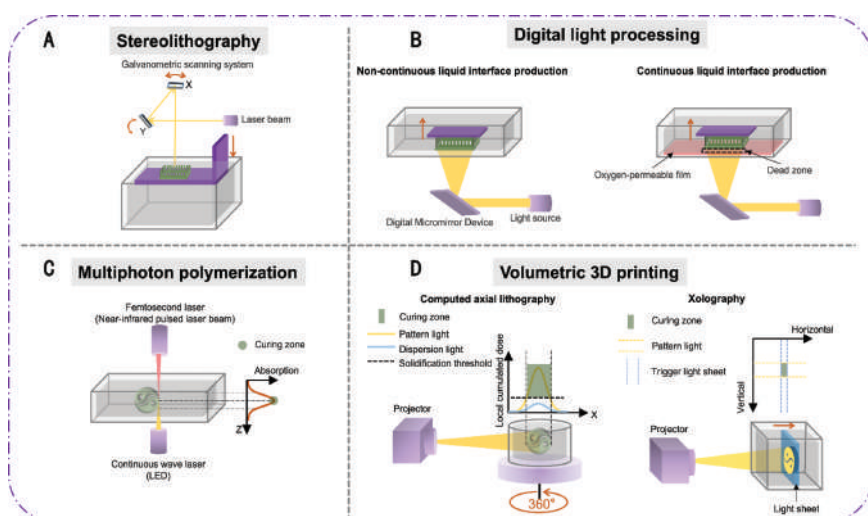


Figure 8.5 Schematics of vat photopolymerization-based 3D printing technologies. (A) Stereolithography. The laser beam focuses on the pre-design position of the platform for horizontally curing the inks, and the Z platform moves for next layer curing. (B) Digital light processing. The digital micromirror device selectively reflects light according to the pre-set pattern for curing the inks, then the Z platform moves for next layer curing. The left technique requires an additional submerging process for replenishing the ink. The right approach avoids the submerging process by introducing an oxygen-permeable film to create the dead zone. (C) Multiphoton polymerization. Two light sources, a femtosecond laser and a continuous-wave laser, overlap as a spot to form the curing zone. As the overlapped spot moves, the pathway gets cured to form structures. (D) Volumetric 3D printing. The dynamic projection of pre-design pattern light is projected to the vat by the projector. For the computed axial lithography, the vat keeps rotating, then the local cumulated dose of exposure within the curing zone increases to reach the solidification threshold for polymerization. For xolography, the curing zone is the overlap area of the trigger light sheet and the pattern light, and the object can be printed by cooperating with the movement of the light sheet.

normally needs a sequential exposure of dissimilar photosensitive materials, and three strategies are adopted to achieve 3D printing of multi-material structures. The first strategy is altering resin by removing the previous materials and replenishing different materials for the next photopolymerization.^{74–76} The other is submerging the semi-product in different vats filled with different materials for the next fabrication.^{77–79} The last strategy is selectively curing the specified material in the vat filled with compound materials by applying different light sources.^{80–82} Figure 8.6 shows the representative application of vat photopolymerization-based 3D printing in multi-component structure fabrication.

8.2.3.1 Stereolithography

SLA, the earliest 3D printing technique, is a laser direct-writing printing method that manipulates a laser beam to cure the photosensitive materials within a vat.^{5,84} With its development, a galvanometric scanning system is integrated to tune the laser beam direction to improve the printing resolution (see Figure 8.5A). During the SLA process, a laser beam passes through the scanning system and then focuses on the surface of the photosensitive ink to sequentially cure. As the previous ink layer is cured, the platform starts to fall to the next layer, and eventually the structure is fabricated in the layer-by-layer photopolymerization. The processing time to print one slice of the structure depends on the scanning speed and the illuminated area.¹⁹ Applying the larger diameter of the spot can shorten the printing time but reduce the printing resolution as the desirable printing resolution of SLA is guaranteed by the spot size of the focused laser beam. Therefore, each exposure dose of the spot, also called the pixel, would theoretically be tuned individually by controlling the laser intensity so that it enables grayscale pattern printing.⁸⁵ Cooperating with sequential exchange and photopolymerization of different materials, SLA allows the fabrication of multi-component structures with multi-materials. Using this method, a six-layer poly-pill containing six drugs was generated by shifting the vats.⁸⁶

8.2.3.2 Digital Light Processing

Curing the resin using a pattern of light seems to be more time-efficient than using the light beam to draw the pattern point by point. Therefore, dynamic mask photolithography has been introduced to the modification of SLA, which contributes to a new type of vat photopolymerization-based printing technique, digital light processing (DLP). In this approach, the digital micromirror device, a dynamic mask made of thousands of micromirrors, is applied to reflect the light source as a pattern light.⁸⁷ During the printing process, the light pattern counterpart is generated according to each slice of structure and projected by the digital micromirror device to selectively crosslink the curable ink to form the final structure layer by layer (see Figure 8.5B). Before crosslinking the next layer, uncured ink between the

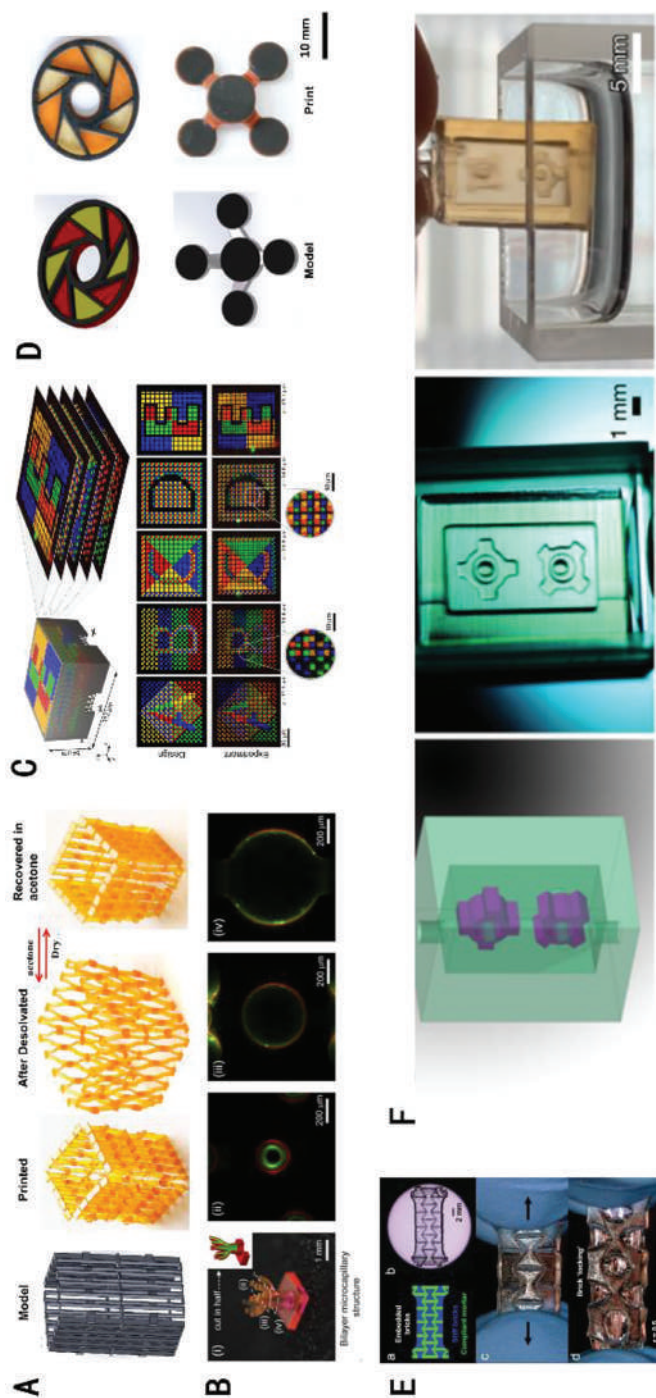


Figure 8.6 Representative examples of vat photopolymerization-based 3D printing. (A) 3D self-expansion/shrinkage structure printed by gray level printing. Adapted from ref. 83 with permission from IOP Publishing, Copyright 2018. (B) Multi-material bilayer micro-capillary structure printed by alternating materials. Adapted from ref. 74 with permission from Elsevier, Copyright 2019. (C) Structure with multi-color patterns printed by alternating materials. Adapted from ref. 75, <https://doi.org/10.1126/sciadv.aau9160>, under the terms of the CC BY 4.0 license, <https://creativecommons.org/licenses/by/4.0/>. (D) Conductive object with a multi-component structure printed by shifting the vat. Adapted from ref. 77 with permission from Elsevier, Copyright 2017. (E) Soft joints and mechanically reinforced brick-and-mortar structures are printed by a selective curing approach within compound materials. Adapted from ref. 80 with permission from John Wiley & Sons, Copyright © 2018 Wiley-VCH Verlag GmbH & Co. KGaA, Weinheim. (F) Encapsulated flow cell with rotary wheels printed by volumetric printing. Adapted from ref. 20 with permission from Springer Nature, Copyright 2020.

previously cured layer and the light source needs replenishment, and this ink reloading process (dependent on ink viscosity) significantly decreases the efficiency of DLP.⁸⁵ However, due to the one exposure step for each layer, the time needed for processing is still considerably shorter than that needed for SLA in fabricating the complex structure.

Generally, the number of slices composited of the model is one of the essential parameters which tunes the resolution and printing time in 3D printing. As mentioned, the SLA and DLP printing process need replenishment after each layer curing. To shorten the time required for printing high-resolution objects, continuous liquid interface production (CLIP) was developed.¹¹ In CLIP, an oxygen-permeable film is set up in the vat between the surface of the cured layer and the light source to establish a thin uncured liquid layer, called the “dead zone”, where polymerization is inhibited (see Figure 8.5B). Above the dead zone, a vertical mobile platform continuously draws out the cured part from the ink bath, and the resultant suction forces synchronously maintain constant liquid ink replenishment for further curing until completion of the structure. Accompanying the dynamic projected images illuminating the curing surface and the constant ink replenishment, CLIP can obtain smooth objects without slicing traces (using a layer-by-layer approach). However, the fluidity of resin is necessary to support the printing continuity.

8.2.3.3 Multiphoton Polymerization

The phenomenon of absorption of two or more photons is the basis of multiphoton polymerization technology. Theoretically, the simultaneous absorption of two or more photons can occur and contribute to photocrosslinking. Current multiphoton polymerization is mainly processed *via* the two-photon absorption, so we will focus on two-photon polymerization (TPP) in this chapter.⁸⁸ With TPP, the simultaneous absorption of two photons only occurs in the focused spot in which the light intensity is high enough to trigger the polymerization (see Figure 8.5C). A molecule is excited from the ground state (S_0) to an excited state (S_1) by absorbing one photon or to a transient state (S_2) by absorbing two photons within the intermediate virtual state (femtosecond), independently.⁸⁹ The probability of transition depends on the product of the intensities of the two laser beams for TPP.¹⁸ The transition only occurs under a sufficiently high photon concentration so that a tightly focused femtosecond laser beam (~ 780 nm for an fs pulsed Ti:sapphire laser) with high intensity is required. Different from SLA, TPP is a direct laser writing technique in which the laser beam can move in any direction without crosslinking the irrelevant area of resin because most photopolymers are transparent at a wavelength in the near infrared range and the photopolymers will only get cured within the focal volume of two lasers.⁸⁸ As a consequence, the structure is constructed by spatial spot (voxel) in TPP but flat spot (pixel) in SLA. Due to the unnecessary need for ink fluidity for replenishing, high viscosity materials can be applied in TPP. Notably, TPP can generate an overhanging object with a heterogeneous

structure by tuning the crosslinking density of the hydrogel.⁹⁰ For multi-material printing, a multi-layer structure with four materials was printed by cooperating with the microfluidic system where materials can be automatically alternated in the closed vat.⁷⁵ However, the immobilization of the overhanging structure should be concerned in the alternating materials process due to the possible translocation or damage to the structure by the flow.

8.2.3.4 Volumetric 3D Printing

Different from layer-by-layer approaches applied in SLA and DLP printing, the volumetric 3D printing (or volumetric additive manufacturing) technique is proposed to generate an object at once rather than through the sequential addition of building blocks. Computed axial lithography (also known as tomographic 3D printing), a landmark in volumetric 3D printing, is inspired by the image reconstruction procedures of computed tomography.^{79,91,92} In computed tomography, the scanned object is reconstructed by processing a set of X-ray radiographs of the object acquired from various angles with a tomographic algorithm. Inversely, in computed axial lithography, a digital model is first sliced to generate cross-sectional images (voxelization), then a set of projections from 0 to 360 angles are calculated by the tomography algorithm. As shown in Figure 8.5D, each projection propagates through the resin within the vat from a defined angle and the resin solidifies at a specific location (depending on the light intensity) where the superposition of illuminations contributing to the cumulative dose distribution of formed radicals achieves the material threshold (mediated by oxygen inhibition). After rotations, the solidification product can be collected after removing the uncured resin. Due to the unnecessary reflow between the resin and the cured part, this technique allows printing a high-viscosity material with the self-supporting property so that it can be applied for secondary printing with other materials by encapsulating an object inside the vat.⁷⁹

Xolography, a linear volumetric 3D printing technique, is another attractive volumetric printing technique due to its compatibility with high resolution (25 μm) and rapid printing process (four to five orders of magnitude higher than TPP).²⁰ In xolography, two intersection light sources with different wavelengths are leveraged to solidify the localized resin. A sheet of the first light triggers a narrow layer of photoinitiator molecules from the initial dormant state to a latent state (finite lifetime), and subsequently the second light generated by an orthogonal projector focuses sectional slices of the object into the first light plane. In this manner, the polymerization was accurately processed between the second light of the projector and the layer of molecules in the latent state. Incorporating the synchronized movement of the resin vat, a sequence of images is projected for curing, and the structure is continuously fabricated.

8.3 Multicomponent Hydrogels for 3D Printing

8.3.1 General Requirements for Hydrogels in 3D Printing

The requirements for hydrogels to be used in 3D printing depend on the specific techniques. For the extrusion-based approach, the rheological properties of hydrogel materials are important for successful printing. Appropriate rheological properties enable hydrogels to exhibit non-Newtonian properties such as shear thinning and rapid recovery. On the one hand, it helps the hydrogel form filaments that stack on top of each other according to deposition or printing patterns, layer up, and generate high-fidelity 3D structures. On the other hand, it is guaranteed to be squeezed out at a pressure level that maintains cell integrity, reducing cell damage. In addition, the stability of the printed structure over time is another critical requirement for the application of hydrogels in 3D printing, which is closely related to the cross-linking method. Meanwhile, attention needs to be paid to the risk of damage to cells and structural deformation by cross-linking reagents and by-products.

Regarding the droplet jet-based printing approach, mainly referring to inkjet printing and micro-valve printing, the inks are typically required to be less viscous for a smooth ejection. The hydrogel polymer concentration and cell density would synergistically affect the viscosity of the hydrogel for jet-based printing, which has a negative influence on the viability of cells under high shear stress. Moreover, improper formulations are therefore likely to cause problems such as nozzle clogging. The constraints on low ink concentration and cell density can be reduced by employing other jet-based printing techniques, such as acoustic printing, laser-assisted printing, and electrohydrodynamic jet printing, to reduce the influence of shear (see Table 8.1). For example, electrohydrodynamic jet printing can cooperate with micro-valve printing to eject 1% alginate solution to generate tiny droplets, which require larger backpressure resulting in a higher shear force.⁹³ The high resolution and cell viability of jet-based printing make it suitable for printing single cells and DNA materials for studying single cell-level mechanisms and gene transfection.⁹⁴

A mandatory requirement for inks in vat-photopolymerization-based 3D printing is the photo-crosslinkable property, which has the attractive advantages of crosslinking efficiency and spatiotemporal controllability. This could be achieved by using photo-crosslinkable monomers or functionalizing macromolecules with photo-crosslinkable side groups, such as acrylate and methacrylate. During the vat-photopolymerization-based 3D printing process, it is important to control the photoinitiator concentration as too a high dose might result in an entire volume curing and potential toxicity, while a low dose might not be able to polymerize the gel. In a typical digital light processing approach, the ink needs to flow well to refill the layer, while some new processes require weak fluidity. For instance, volumetric printing requires printing materials with high viscosity to minimize the relative

motion between the printed object and the uncured precursor. Kelly *et al.* developed a computed axial lithography (CAL) system that selectively solidifies by volume *via* rotating a vat with photosensitive resins in a dynamically changing light field.⁷⁹

Additional requirements might be issued for hydrogels being used in biomedical applications. For example, 3D bioprinting usually involves the use of cellularized bioinks. Due to the involvement of living cells in the 3D printing process, balancing structural printability with cell viability and bio-functionality still has lots of challenges. For example, printability can be optimized by increasing polymer concentration in the single-component hydrogel, but the resulting stiff microenvironment and dense polymer networks might hinder important cellular processes such as proliferation, differentiation, and extracellular matrix (ECM) deposition.⁹⁵ Thus, the single-component hydrogel is unlikely to meet the comprehensive requirements in 3D printing, especially 3D bioprinting. The development of inks based on multicomponent hydrogels has become more attractive. In the following sections, we will review the most recent advances in multicomponent hydrogels used in 3D printing and categorize them into miscible and immiscible systems (see Table 8.2).

8.3.2 Miscible Multicomponent Hydrogels in 3D Printing

8.3.2.1 Multi-material Hydrogels

A single material is challenging to meet the composite demands of 3D printing structures, and their properties, so miscible multi-material hydrogels are prepared from mixtures of two or more miscible polymer solutions (see Figure 8.7A). This is a straightforward way to combine the advantages of different materials. For example, the gelatin–alginate hybrid hydrogel is a typical multi-material hydrogel applied in 3D printing, where the thermogelation of gelatin mediates the extrusion-based printability, and ionic crosslinking of alginate stabilizes the printed constructs during physiological incubation.^{110,111} In the selection of polymers, it is often possible to divide and combine natural polymers and synthetic polymers, which have different characteristics. In biomedical applications, natural polymers, especially those derived from the ECM, are generally preferred over synthetic polymers in the design of ink formulations due to their better biocompatibility, biodegradability, cell affinity, and ability to mimic natural ECM properties. Sodium alginate, hyaluronic acid, fibrin, and collagen are parts of the representative natural polymers that can promote cell growth and differentiation. However, these natural hydrogels usually exhibit poor mechanical properties and structural integrity and thus are limited in biomedical applications. Synthetic polymers offer advantages such as well-defined chemistry, good mechanical properties, and tunable degradation rates, but usually exhibit poor biocompatibility. Formulating these polymers into multimaterial hydrogel inks would likely address the challenges issued to individual types.

Table 8.2 Examples of different types of multicomponent hydrogels used in 3D printing.

Category	Types of multicomponent hydrogels	Examples	Crosslinking mechanisms between multi-components	Advancements	Ref.	
Miscible multicomponent	Multi-material	PU-gelatin	Hydrogen bonds	Enhanced and tunable mechanical properties	96	
		Methacrylated hyaluronic acid (HAMA)-GelMA		Printed heart valve for cellular and encapsulated environment interactions	97	
		Polyethylene glycol (PEG)-PEG crosslinkers (PEGX)	Amine-carboxylic acid	Expanded and customizable biomaterial palette	98	
	Interpenetrating network	Alginate-GelMA	Electrostatic interaction, radical polymerization	Improved printability with low concentration GelMA solutions	99	
		Alginate-PEG	Electrostatic interaction, radical polymerization	Highly stretchable and tough properties	100	
		Polyvinylpyrrolidone (PVP)-silk fibroin (SF)	Electrostatic interaction, radical polymerization	Highly light transmission, fast sol-gel transformation	101	
	Supramolecular	Hyaluronic acid (HA)	Guest-host	High-resolution patterning of multiple inks, cells, and void spaces	163	
	Immiscible multicomponent	Aqueous two-phase	PAA-dextran (DEX)/polyethylene oxide (PEO) GelMA-PEG	Hydrogen bonds	Enabled reconfigurable embedded all-liquid architecture	102
		Nanocomposite	Collagen-nanosilicate	Hydrogen bonds	Unique biocompatible miscible aqueous system	103
			Alginate-nano-hydroxyapatite (NHA)-pDNA-PCL	Electrostatic interaction	Improved mechanical properties and function on regeneration of bone in nonunion defects	104
		GelMA-gold nanorod (GNR)	Electrostatic interaction	Successful cell transfection and differentiation on bone defect regeneration	105	
Microphase-incorporated		Gelatin microgel template pore gel - a series of complementary networks	Electrostatic interaction	Improved cell adhesion and synchronized contractility for printed cardiac tissue	106	
		Carbon nanotubes (CNTs)-PEGDA	Hydrogen bonds	Simple and expanded strategies for constructing precise micropores	107	
	45S5 bioactive glass (BG)-alginate dialdehyde (ADA)-gelatin (GEL)	Electrostatic interaction	Promoted neurite outgrowth under electrical stimulation	108		
		Covalent bonds and ionic gelation	Enhanced mechanical properties and promoted osteogenic expression	109		

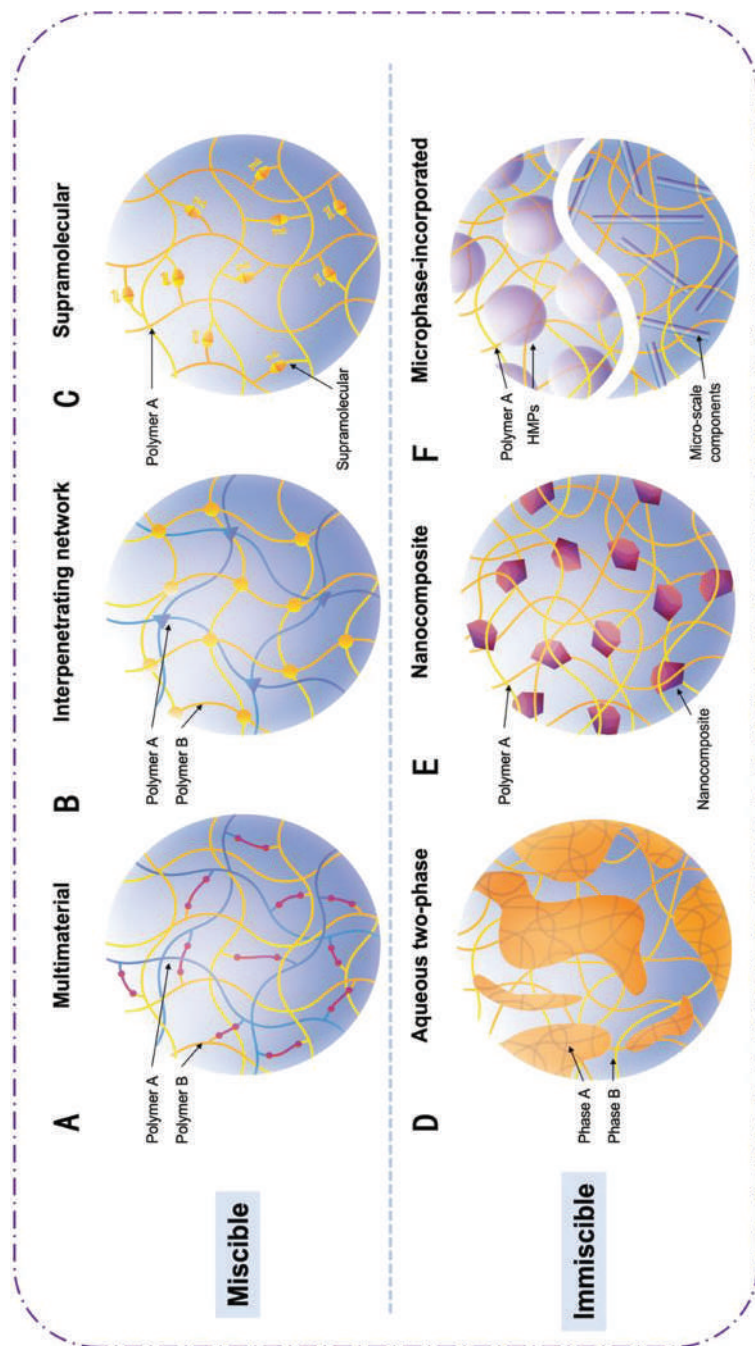


Figure 8.7

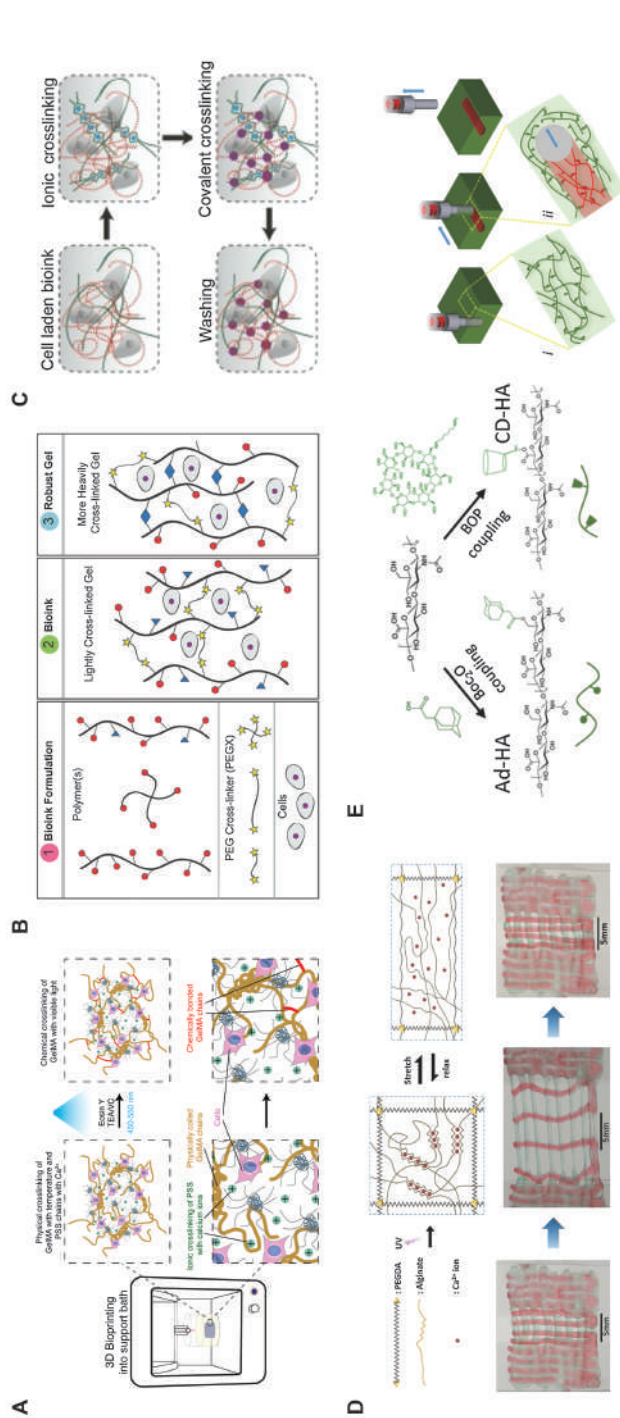
Schematics of strategies for formulating multicomponent hydrogels in favor of 3D printing. (A) Multimaterial hydrogels. Two or more polymer networks are tightly connected by specific chemical interactions. (B) Interpenetrating network hydrogels. Only physical entanglement occurs between two or more polymer networks. (C) Supramolecular hydrogels. Dynamic connections between polymer networks, including multiple hydrogen bonds, van der Waals interactions, host-guest interactions and electrostatic interactions. (D) Aqueous two-phase hydrogels. Hydrogels contain two immiscible water-phase materials that tend to have similar densities. (E) Nanocomposite hydrogels. Nanoscale particles are added to continuous phase materials to enhance mechanical strength or introduce special functionalities. (F) Microphase-incorporated hydrogels. Microscale dopants include hydrogel microparticles or other micro-scale components such as bioglass and microcarriers.

The crosslinking mechanisms of inks are critical for the 3D printing process.³¹ Thermally responsive hydrogels, such as gelatin, poloxamer, agarose, and Matrigel, are popular candidates to formulate a multi-material ink owing to the simple gelation. Gelatin is a denatured product of collagen, a low charge density peptide polymer. It is well known for its significant temperature sensitivity. It should be noted that it is difficult to determine a strict temperature of melting and gelling points, which vary from different gelatin sources and processing methodologies. Gelatin from cold-water fish possesses significantly lower gelling and melting temperatures (4 to 12 °C and <17 °C, respectively) than the porcine and bovine gelatin does.^{112,113} Recently, we developed a complementary network bioink system based on gelatin and a series of photocrosslinkable components.¹¹⁴ Gelatin mediates the thermoresponsibility, and the other complementary component stabilizes the printed constructs for subsequent incubation under physiological conditions. This generalizable approach allows for the standard 3D printing of various hydrogels with a wide range of compression modulus from ~1 to ~200 kPa.

To better suit the 3D printing process, many polymers can be modified with functional side groups to mediate structural printability and biomedical functionality. Photocrosslinking is an attractive property due to its accurate spatial and temporal control of gelation, highly tunable physical properties, and fast reaction. GelMA is an excellent photo-crosslinkable ink candidate, which exhibits biocompatible photo-crosslinking properties, thermal responsivity, unique biofunctionality, a fast gelation process, anti-inflammatory activity, and mechanical stability. For example, GelMA and poly(3,4-ethylenedioxythiophene) (PEDOT):poly(styrenesulfonate) are mixed to prepare a conductive ink formulation being used in both wet spinning and 3D printing methods (see Figure 8.8A).¹¹⁵ The fabrication process was performed through an initial crosslinking step with divalent calcium ions and a secondary photopolymerization step with visible light, with a resulting Young's modulus of 40–150 kPa. To expand the universality of ink formulations, Rutz *et al.* designed bioinks based on multifunctional PEGX by combining different polymers, including linear (*e.g.*, gelatin), branched (*e.g.*, 4-arm PEG amine), or multifunctional (*e.g.*, GelMA) polymers (see Figure 8.8B).⁹⁸ The PEGX cross-linker provides the necessary viscosity and post-printing support by covalently bonding other low-concentration polymers that favor cell encapsulation and culture.

8.3.2.2 Interpenetrating Network Hydrogels

IPN hydrogels are formed by the entanglement of at least two cross-linked networks, which could usually enhance the mechanical properties as single-network hydrogels are often weak, especially in the field of tissue engineering (see Figure 8.7B). Theoretically, there is little chemical interaction between the different polymer networks in IPN hydrogels. A well-known subset of IPN hydrogels is double-network (DN) hydrogels. Gong *et al.*



reported a DN hydrogel prepared from two synthetic polymer networks, namely poly(2-acrylamido-2-methylpropanesulfonic acid) (PAMPS) and poly(acrylamide) (OAAm).¹¹⁶ The resulting hydrogel shows high strength, sustaining a stress of 17.2 MPa and a fracture strain of 92%. The DN hydrogel is composed of two separate cross-linked networks, in which the main feature is the incorporation of a flexible neutral second polymer network into a swollen rigid and brittle first polymer network. It is the reason that DN hydrogels usually exhibit better mechanical properties than general IPN hydrogels. However, the formation of typical DN hydrogels is slow and might face difficulties when applied to 3D printing because the secondary polymer monomers need to be completely dispersed in the primary network, which is usually covalently cross-linked. Some studies have chosen to crosslink the first polymer network with metal cations since ion penetration and crosslinking can proceed simultaneously with covalent second polymer network formation.¹¹⁷ Many sub-categories of IPN hydrogels are derived from the different cross-linking methods of the multi-layer polymer network. For the convenience of understanding, the following are all described in terms of IPN.

Alginate, a natural ionic polysaccharide isolated from brown algae, is one of the ideal hydrogels as the primary polymer within IPNs because it could be crosslinked and dissociated by multi-cations easily.¹¹⁸ Acting as a structural template, the inert alginate hydrogel can properly keep the printed multilayer structure from collapsing. The lack of cell adhesion ligands in alginate drives researchers to combine it with bioactive polymer networks in order to introduce both structural fidelity and biocompatibility to the printed structures.¹¹⁹ Colos *et al.* developed a low-viscosity bioink (4.5% w/v GelMA) made of alginate and GelMA to print homogeneous HUVEC-loaded fibers (see Figure 8.8C).⁹⁹ In detail, it was found that the viscosity of the alginate/GelMA mixture was reduced three times that of pure alginate, and at the same time weak temperature sensitivity was observed, which improved the self-heating gel of GelMA. Hong *et al.* constructed a network with sodium alginate and poly(ethylene glycol) (PEG) and bioprinted highly stretchable and tough hydrogels tougher than natural cartilage.¹⁰⁰ The hydrogels showed excellent stiff and ductile performance attributed to mechanical energy dissipation of the reversible alginate network and high elasticity of the covalent PEG network (see Figure 8.8D). In some studies, alginate was retained as a support structure after ionic cross-linking, while the other components in the composite bioink were not cross-linked and might dissolve out to form pores over time, beneficial to control the properties of the printed scaffolds more precisely, such as porosity, water absorption, and mechanical properties.¹²⁰

SF is an attractive option when developing IPN hydrogel inks owing to its good biocompatibility, well-controlled degradability, versatile processability, and remarkable pro-osteogenic properties.¹²¹ However, the application of silk fibroin hydrogels in extrusion-based 3D printing is limited by their low viscosity.¹²² Mixing other high-viscosity biomaterials or rheological

modifiers is a convenient and straightforward strategy to improve its printing processability and biofunctionality. Wen *et al.* used a UV-curing method to develop an IPN bioink with a polyvinylpyrrolidone (PVP) and SF macromolecular hydrogel. The bioink has nearly 100% light transmission and fast sol-gel transformation.¹⁰¹ Maleki *et al.* developed an ultralight nano-silica-SF IPN aerogel mixture to obtain micron-scale honeycomb topological pores ($\sim 0.5\text{--}18\ \mu\text{m}$) for bone scaffolds by unidirectional freeze-casting and CO_2 supercritical drying.¹²³ Among them, SF has high mechanical elasticity, which supports the compression and bending flexibility of printed bone scaffolds as ECM, which also positively affects the viscoelasticity and swelling/deswelling properties of IPN hydrogels.

8.3.2.3 Supramolecular Hydrogels

Hydrogels for tissue engineering applications are usually required to be strong enough to withstand deformation cycles and reduce loss of mechanical integrity. To achieve these properties, supramolecular hydrogels have been developed, which combine the reversibility of physical bonds with the versatility and customizability of covalent bonds (see Figure 8.7C). When subjected to cyclic stress, the dynamic bonds in a supramolecular hydrogel can be temporarily broken. This break is reversible and can be rapidly reformed again. Such properties are beneficial during extrusion-based printing to achieve ‘shear-thinning’ behavior, which suggests a gel-sol transition in response to external mechanical stimuli.¹²⁴ When applying shear stress to a supramolecular ink, the decrease of the gel modulus makes it flow during the injection process (loss modulus $G'' >$ storage modulus G'). However, upon removal of the shear force, the storage modulus recovers rapidly by the reformation of physical cross-linking.¹²⁵ Applying supramolecular principles to the gel mechanism of hydrogels can simulate dynamic non-covalent interactions in natural matrix materials, including multiple hydrogen bonds, electrostatic interactions, van der Waals interactions, and host-guest interactions. It enables biomimetic dynamic reciprocity, providing spatio-temporal control over biological activity, chemical composition, and mechanical properties.¹²⁶

In particular, the dynamic properties of supramolecular bioinks are attractive for extrusion-based bioprinting, which enables the rapid and stable construction of complex structures. The main design goals of supramolecular polymers are to accelerate the self-healing speed and increase the viscosity and elastic modulus of the ink.¹²⁷ Such properties required for DIW polymers can be improved by introducing metal-ligand coordination networks and host-guest auxiliaries, such as establishing multivalent coordination between the carboxylate groups of alginate and calcium ions. Chemical modifications are usually needed to introduce supramolecular properties to biopolymers. For example, HA is a linear non-sulfated proteoglycan that plays a lubricating role in connective tissue and has high water absorption and retention capacity. To form a proper hydrogel, HA is

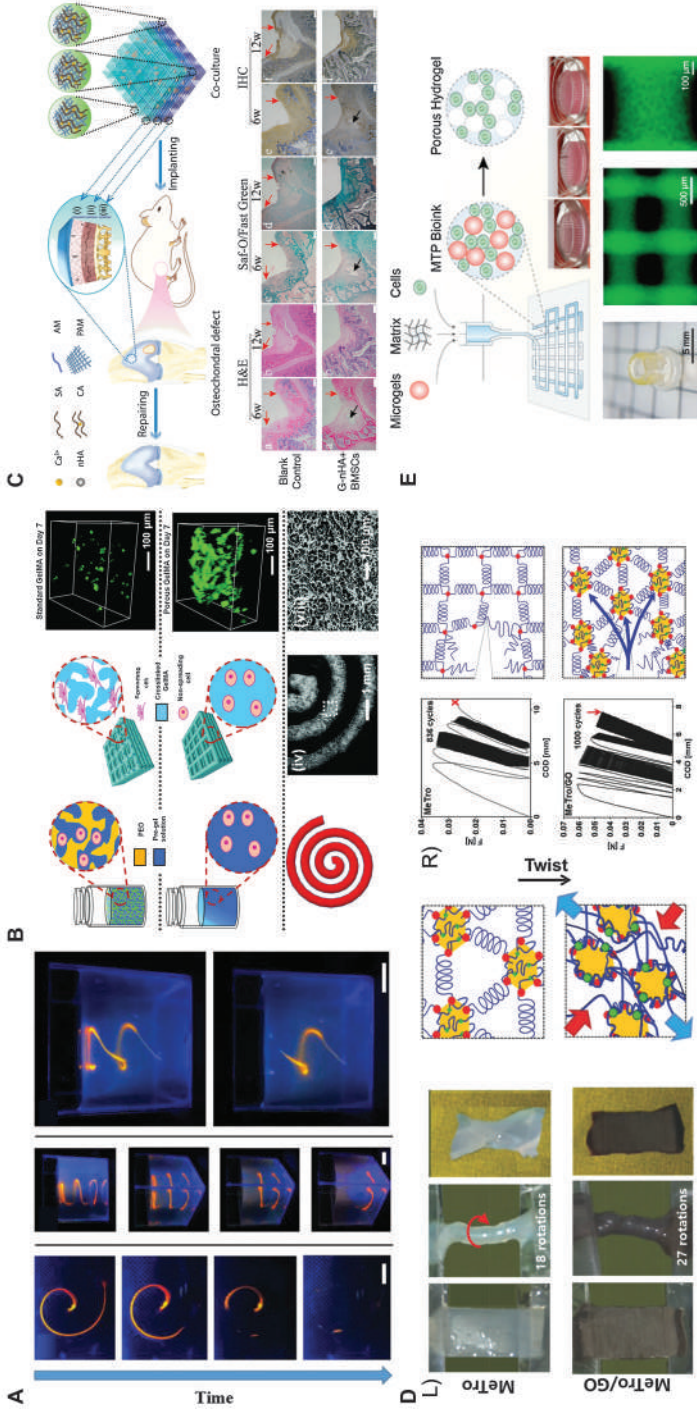
commonly modified with methacrylate (the resulting material is HAMA), which allows for covalent photocrosslinking in the presence of a photoinitiator and light. Burdick's group further introduced guest–host chemistry to HAMA and developed a robust injectable and printable formulation.¹²⁸ Specifically, they coupled adamantane and β -cyclodextrin groups to HAMA and achieved self-assembled hydrogels due to the guest–host interaction between Ad and CD groups. Highley *et al.* reported the direct printing of HA–Ad and HA– β -CD polymers with methacrylate groups as inks into self-healing supported hydrogels for bioprinting applications.¹⁰² The two-fold supramolecular hydrogels are dynamically equilibrated in mutual contact, allowing the specification and printing of various hydrogel structures (materials, voids, and cells) at high resolution in a given three-dimensional space (see Figure 8.8E).

8.3.3 Immiscible Multicomponent Hydrogels

8.3.3.1 Aqueous Two-phase Hydrogels

An aqueous two-phase system (ATPS) refers to the appearance of two immiscible phases when two aqueous solutions containing appropriate concentrations of certain polymers or salts (either lyophilic or chaotropic) are mixed (see Figure 8.7D).¹²⁹ The phase separation is due to the thermodynamic incompatibility of the two polymers.¹³⁰ In this system, the entropy contribution is less than the enthalpy contribution, so the free energy is greater than zero, resulting in phase separation. In addition, the small difference in density between the two polymers creates an extremely small interfacial tension, allowing the two phases to mix, albeit immiscibly.¹³¹ ATPS is promising in the field of tissue engineering, especially bioprinting, because a fully aqueous environment is prominently favourable for cell printing and survival. It is also possible that the use of ATPS improves the stability and ease of tunability of printing parameters, as phase separation enables two-phase control in the ink over a wide range of temperatures, phase volumes, mass fraction ratios, and osmotic pressure.¹³²

ATPS has shown significant prospects in terms of tissue engineering, ranging from 2D bio-patterning to 3D bioprinting. The former application is more established, usually by depositing cell-rich DEX aqueous droplets onto PEG-rich aqueous substrates to generate cell islands or colonies.¹³³ The ultra-low interfacial tension of the two-phase interface provides a very mild ecological niche for cell culture. Cell micropatterning has also been extended to high-throughput three-dimensional (3D) platforms. It opens a window to the study of cell–cell interactions, such as the direct impact of adjacent cell types,¹³⁴ cell density,¹³⁵ and colony size on neural cell differentiation.¹³⁶ Furthermore, the introduction of ATPS is attractive for developing embedded 3D bioprinting for spatially free-defined tissue construction, where the printed shape is preserved through the formation of interfacial coacervates. PEO and DEX systems have been shown to have



hydrogen bond interactions to generate complex, free-form 3D all-liquid structures and preserved for more than ten days, with a considerable survival rate of NIH 3T3 fibroblasts (90%).¹³⁷ Immiscible PEG and dextran solutions are another typical ATPS, and aqueous tubules can be printed in water to observe selective ion separation and accumulation (see Figure 8.9A).¹³⁷ Furthermore, ATPS-based bioinks could be used to prepare porous hydrogels by sacrificing the discontinuous phase, with the advantage of tunable pore size. Discontinuous PEO droplets were dispersed in the continuous GelMA phase, leaving tens of micrometers of voids removed by soaking in PBS for 24 h.¹⁰³ GelMA and PEG constitute an unusual bicontinuous state of aqueous two-phase dispersions in which the GelMA phase encapsulates living cells and rapidly photocrosslinks to form hydrogel sponges after removal of the uncrosslinked PEG phase (see Figure 8.9B). The continuous microtubule structure in this sponge can be generated simultaneously upon gelation, potentially chemically and structurally mimicking a tightly packed capillary network, although precise control of pore size and homogeneity might be difficult.

8.3.3.2 Nanocomposite Hydrogels

Nanocomposite hydrogels contain nanomaterials in different forms, including nanoparticles, nanodisks, and nanofibers (see Figure 8.7E). The introduction of some nanomaterials, including graphene, graphene oxide,

Figure 8.9 Examples of immiscible multicomponent hydrogels. (A) Optical images showing a PAA-DEX two-phase hydrogel 3D-printed in an all-aqueous environment under UV light irradiation, allowing erasure and modification. Adapted from ref. 137 with permission from John Wiley & Sons, Copyright © 2019 Wiley-VCH Verlag GmbH & Co. KGaA, Weinheim. (B) Two-phase porous hydrogel constructs of immiscible GelMA and PEO for culturing NIH/3T3 fibroblasts and 3D printing compared to the conventional GelMA hydrogel. Adapted from ref. 103 with permission from John Wiley & Sons, Copyright © 2018 Wiley-VCH Verlag GmbH & Co. KGaA, Weinheim. (C) Schematic of a 3D printed gradient NHA multilayer nanocomposite hydrogel scaffold. Histological and immunohistochemical analyses of the osteochondral (OC)-deficient areas of the seven groups of grafts demonstrated the best cartilage defect repair effect in the “G-NHA + BMSCs” group. Adapted from ref. 138 with permission from John Wiley & Sons, Copyright © 2020 Wiley-VCH GmbH. (D) Images and schematic diagrams of the torsion test (L) and cyclic tensile test. Adapted from ref. 139 with permission from John Wiley & Sons, Copyright © 2015 Wiley-VCH Verlag GmbH & Co. KGaA, Weinheim. (R) The high elasticity of the MeTro/graphene oxide (GO) highly elastic hybrid hydrogel, compared to the pure MeTro hydrogel. (E) A tunable microgel template pore gel for 3D printing, where the porosity of the printed structures is evidenced by confocal images. Adapted from ref. 107, <https://doi.org/10.1002/adhm.202200027>, under the terms of the CC BY 4.0 license, <https://creativecommons.org/licenses/by/4.0/>. Scale bars: A = 10 mm.

CNTs, hydroxyapatite, BG, and calcium phosphate, can enhance mechanical and physicochemical features, and improve biological and functional properties.¹⁴⁰ Usually, the improvement effect is positively correlated with the content of particles. Some studies have mentioned that the addition of inorganic nanoparticles (*e.g.*, gold nanomaterials, nanosilicates, *etc.*) can improve cell adhesion, organization, diffusion, and/or differentiation within the printed structures to some extent. A recent study incorporated aminated mesoporous BG nanoparticles into a composite hydrogel based on ADA-GEL for 3D printing in order to introduce osteogenic differentiation and angiogenesis. The introduction of dynamic covalent chemistry between hydrogel chains and nanoparticles likely engineers a dynamic microenvironment for embedded cells, leading to enhanced cellular function.¹⁴¹

Synthetic silicate clays offer great potential for bioprinting applications. It has a highly negatively charged surface and positively charged edges that can generate shear-thinning properties through electrostatic interactions with polymers. The resulting self-assembled structures can dynamically form and break. Xavier *et al.* developed collagen-based hydrogels containing two-dimensional nanosilicates.¹⁰⁴ Notably, the addition of nanosilicate decreased the degree of hydration and significantly enhanced the mechanical stiffness, perhaps due to the strong interaction between the nanosilicate and the gelatin substrate. The inclusion of 2% nanosilicate increases the compressive modulus by a factor of 4 and also increases the peak tensile stress by a factor of 10 at 90% strain.

NHA is abundant in native calcified cartilage or subchondral bone and is therefore widely used in the construction and transplantation of OC composites. Studies have shown that it is critical for the differentiation of BMSCs into osteoblasts, accelerating subchondral bone formation, and promoting the interface between bone and hyaline cartilage. Zhang *et al.* added NHA to a DN hydrogel scaffold with OC-like tissue structures based on sodium alginate and acrylamide.¹³⁸ Although alginate by itself better supports hyaline cartilage development, as evidenced by type II collagen tissue staining, the results showed that the NHA-incorporated group had the best repair effect on the OC defect, and the corresponding microstructure of cancellous bone was similar to that of natural tissue (see Figure 8.9C).

Conductive nanomaterials, such as carbon nanotubes, graphene oxide, and gold nanoparticles, have unique mechanical, electrical, and biological properties for a diversity of biomedical applications (see Figure 8.9D).¹³⁹ For example, gold nanoparticles can induce cardiomyocyte maturation in 3D cardiac tissue architecture and organization. Zhu *et al.* developed a GNR-based GelMA bioink for printing 3D functional cardiac tissue structures.¹⁰⁶ At the optimized GNR concentration, the nanocomposite bioink has a low viscosity similar to the pristine ink, which can reduce the shear stress on the encapsulated cells. The experimental results indicate that the Mion G-GNR/GelMA hydrogel provides a beneficial microenvironment for cardiomyocyte retention, growth, and function.

8.3.3.3 Microphase-incorporated Hydrogels

Hydrogel microparticles (HMPs) are typically used to engineer microphase-incorporated hydrogels (see Figure 8.7F). In the packed or plugged state, HMPs connect and support each other through interactions that are weaker than covalent bonds, while they can still retain the macrostructure to a certain extent. On the other hand, the generated formulation can flow when external forces overcome interparticle friction, thus possessing the shear-thinning properties required for 3D printing. The advantage of HMPs is that the microgels are not destroyed during shear flow and can potentially protect the encapsulated cells from high shear stress.¹⁴² Feng *et al.* assembled microgel particles ($\approx 100 \mu\text{m}$) through a dynamic cross-linking reaction, which improved the dynamic viscosity and maintained a relatively low mechanical modulus.¹⁴³ Another use of HMPs is to introduce controlled micropores into the hydrogel, which could lead to a more biomimetic microenvironment for tissue engineering. For example, we recently reported a tunable microgel template pore gel bioink system, and the microgel size can be as small as 10–100 μm .¹⁰⁷ Such microgel-containing hydrogels can be engineered with controllable porosity (up to 70%) and small pore size in building blocks for the fabrication of porous scaffolds (see Figure 8.9E).

The weak mechanical properties of hydrogels significantly limit their application as load-bearing biomaterials as required in artificial cartilage and tendons. Micro-scale immiscible particle components are often used to enhance hydrogel networks to obtain composites with superior mechanical and biological properties or tailored functionalities (see Figure 8.7F). SF-based hydrogels have good biocompatibility and can be used to obtain stiff hydrogels. Kim *et al.* developed a methacrylated SF hydrogel for digital light processing bioprinting.¹⁴⁴ In addition, some micro-sized dopants are often encapsulated in non-covalent physical DN hydrogels, which have significant self-healing properties compared to covalent DN hydrogels, further enhancing the mechanical behavior. Hou *et al.* introduced macromolecular microspheres into DN hydrogels as the physical cross-linking centers of the hydrophobic segments so that the hydrophobic monomer hexadecyl methacrylate was stably adsorbed to the surface of microspheres, forming a second-layer network entangled with the primary gelatin network.¹⁴⁵ Microsphere-based DN hydrogels exhibit up to 2100% fracture strain and dynamic fatigue resistance.

8.4 Biomedical Applications of 3D Printed Multicomponent Hydrogels

8.4.1 Tissue Engineering and Regenerative Medicine

Tissue and organ damage within the human body can occur due to injury or diseases. The affected body parts can only benefit from a limited ability to repair, self-renew, or regenerate.¹⁴⁶ In addition, traditional approaches

(e.g., allograft, xenograft) to replacing the affected body part face a variety of challenges, such as donor shortage and body immune rejection. Tissue engineering approaches have provided more opportunities for regenerative medicine and are becoming more and more important as they represent a way to overcome the described challenges.¹⁴⁷ For example, a multicomponent hydrogel of gelatin, fibrinogen, HA, and glycerol is used in conjunction with stem cells extracted from human amniotic fluid to fabricate a mandibular bone fragment for a patient. Using a self-developed extrusion-based bioprinting system, ITOP, which enables microchannel inclusion and facilitates the manufacturing process, the bone fragment is fabricated.²¹ In addition to properties to ensure cellular viability, the multicomponent hydrogel features calcium deposition capability. The 3D printing of cartilage tissue represents another broad application spectrum. The elastic connective tissue holds a high potential for the use of additive manufacturing processes, as it does not contain nerves and blood vessels and contains only one cell type. The challenges lie in the different depth composition gradients and the strong heterogeneity of cartilage tissue. In one approach, a multicomponent hydrogel of gellan and alginate is used in combination with cartilage ECM particles so that high-resolution cartilage grafts with sufficient biological and mechanical requirements can be produced. These can be customized to the patient and used for noses, vertebral disc grafts, or ears.¹⁴⁸

Osteochondral tissue engineering represents another important application area for the 3D printing of multicomponent hydrogels (see Figure 8.10B). Osteochondral defects, which include both the articular cartilage and the underlying subchondral bone, can lead to functional limitations of joints and cause severe physical pain in the patient. To overcome the limitations of current treatment methods, engineering an osteochondral

Figure 8.10 Examples of applications in tissue engineering and regenerative medicine. (A) Fluorescence and light micrographs of *in situ* endothelialization. HUVECs were seeded on 3D channels. Adapted from ref. 153, <https://doi.org/10.1002/adfm.201908349>, under the terms of the CC BY 4.0 license, <https://creativecommons.org/licenses/by/4.0/>. (B) Schematic illustration of tissue substitutes for multi-layered osteochondral defects *via* 3D printing (left) and structure of multi-channel 3D printing of artificial full-thickness osteochondral plugs based on a hydrogel (red) and a calcium phosphate cement (white). Adapted from ref. 154, <https://doi.org/10.1038/s41598-020-65050-9>, under the terms of the CC BY 4.0 license, <https://creativecommons.org/licenses/by/4.0/>. (C) (a) Schematic of the design for a 3D bioprinted multichannel scaffold for modeling the spinal cord. (b) Overview of the 3D bioprinting process. (c–f) Structure of the multichannel scaffold of the spinal cord. Adapted from ref. 152 with permission from John Wiley & Sons, Copyright © 2018 Wiley-VCH Verlag GmbH & Co. KGaA, Weinheim. (D) Placement and size distribution of 3D bioprinted islet tissue. Adapted from ref. 151 with permission from John Wiley & Sons, Copyright © 2019 Wiley-VCH Verlag GmbH & Co. KGaA, Weinheim.

composite tissue substitute is an option.¹⁴⁹ One example describes the development of a multilayer osteochondral alternative tissue using an extrusion-based 3D printer. The composite tissue is divided into three distinct zones, which consist of a mineralized biomaterial phase as well as a multicomponent hydrogel loaded with human chondrocytes or mesenchymal stromal cells. A multicomponent bioink composed of alginate and methylcellulose is used, where alginate is used to realize chondrogenesis, the process of cartilage formation. However, when used alone, alginate does not achieve high enough viscosity for good shape retention in extrusion printing, so methylcellulose is added. The resulting composite bioink allows for cell encapsulation with considerable cell viability and metabolic activity and good printability that can produce sufficiently precise 3D constructs.¹⁵⁰

Apart from bone and cartilage, 3D printed hydrogels can be used to treat other tissues with diseases. One approach describes a procedure involving the metabolic disease diabetes. During the course of the disease, the insulin-producing islet cells in the pancreas are attacked by the immune system, and their function is impaired (see Figure 8.10D). Difficulties occur after transplantation in the form of dwindling islet mass and islet function. To overcome the difficulties, the cells are encapsulated in a hydrogel matrix to increase cell function and survival capabilities. The hydrogel matrix consists of high-purity alginate and methylcellulose and is printed using a 3D extrusion bioprinter. The use of a multicomponent hydrogel in the form of different alginates leads to a plottable mass characterized by a high fidelity of the printed scaffolds. The results show high potential to increase survivability, ensure functionality, and preserve islet cell morphology within the hydrogel for seven days.¹⁵¹ In another example, researchers address the treatment of neurological diseases, such as spinal cord injuries, by developing patient-specific clinical implants using bioprinting¹⁵² (see Figure 8.10C). The 3D printed construct is made of a combination of Matrigel, gelatin/fibrin, and GelMA and a cell mixture of oligodendrocyte progenitor cells and derived spinal neural progenitor cells. The custom-made 3D cellular scaffold is characterized by stable contact with the native spinal cord. The potential for successful treatment of neurological diseases by bioprinting can be confirmed by intracellular calcium flux studies by confirming the viability and functionality of the neural progenitors.

The use of several combined hydrogels as ink materials holds huge optimization potential in the field of tissue engineering and regenerative medicine, as the described examples have already illustrated. In addition, further versatile application examples exist on various parts of the human body. The primary challenge with respect to multicomponent hydrogel inks is the recapitulation of the unique anatomy in the form of intricately branched, sometimes multi-layered structures. This challenge can be overcome by mimicking the environment as closely as possible in the form of different cell types and ECM microstructures while incorporating external parameters. The field has also evolved tremendously with the advances in 3D printing. We can envision that there will be more technological

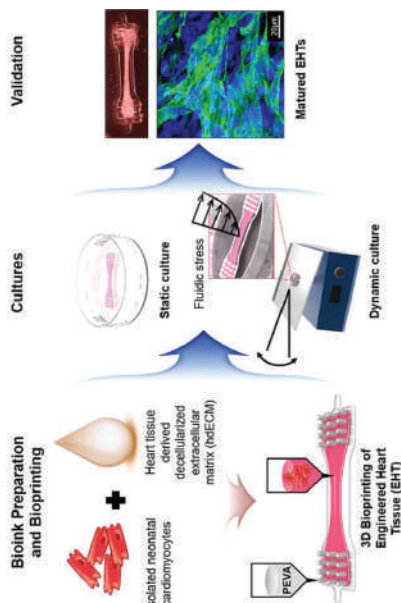
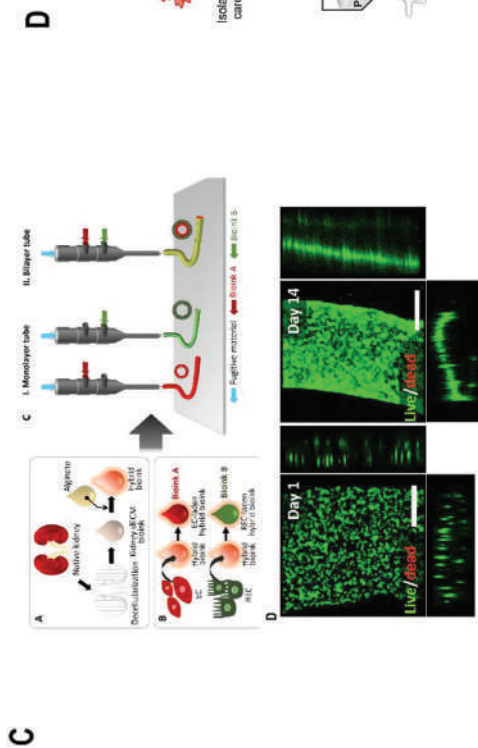
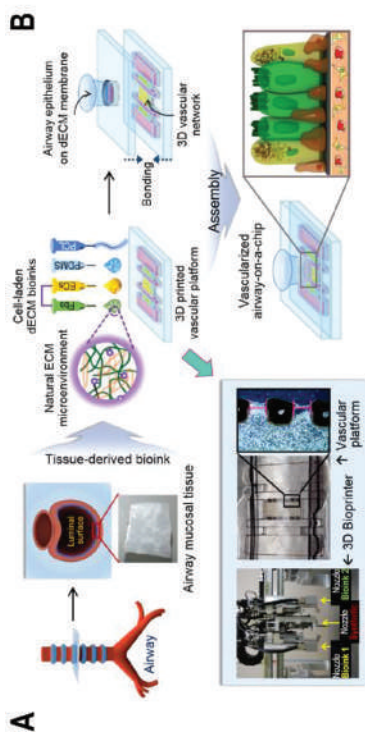
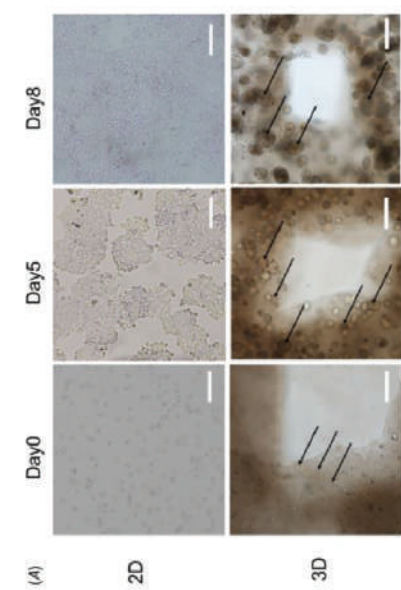
breakthroughs, and products that are clinically applicable might make their appearance before too long. However, to keep up with this progress, external circumstances such as patient acceptance, legal regulations, and the willingness of health insurance companies to pay must also be taken into account.^{150,152}

8.4.2 Disease Modeling and Drug Testing

Conventional treatments of diseases are based on the “one-size-fits-all” approach and show only moderate success in certain disease processes, such as cancer. The response to therapies and the patient’s quality of life in difficult-to-evaluate species are variable because disease patterns are highly individualized. For this reason, 3D printing disease models that can map complex and heterogenous intercellular and cell–matrix interactions, drug screening, and the creation of patient-specific treatment regimens are among those being produced.¹⁵⁵

Cancers are second only to cardiovascular diseases on the list of the most frequent causes of human death and can also impose a heavy economic burden on the patient. An initial study in extrusion-based bioprinting of cancer cells was performed by Xu *et al.* in 2010.¹⁵⁶ One approach focuses on the development of breast cancer models using extrusion bioprinting. The spheroid bioprinting model is based on patient-derived MCF-7 breast cancer cells and a hydroxyethylcellulose/alginate/gelatin hydrogel.¹⁵⁵ This approach represents a promising approach in terms of developing personalized breast cancer therapy and opens new possibilities in drug screening. Furthermore, a unique feature of the 3D bioprinting approach worth highlighting is the ability to precisely deposit the multicellular microenvironment, which is composed of the ECM, the interstitial fluid, and the cells themselves, and thus fabricate the model.¹⁵⁷ The modified extrusion method, such as coaxial extrusion, was demonstrated to fabricate a multicellular tumor model.¹⁵⁸ Also, vat photopolymerization-based 3D printing was utilized to form the microenvironment, like the bonelike microenvironment or high-resolution microchannels (<25 μm), and to study the behavior of cancer invasion in these microstructures.¹⁵⁹ Droplet jet-based 3D printing is another bioprinting methodology to form tumor tissues with faster speed and high resolution.¹⁶⁰ Bioprinting can also allow the production of multiple scales of the vasculature, such as coaxial printing or cooperation of sacrificial material supporting and bioprinting, enabling the growth of larger tumor organoids.^{161,162}

Sometimes single cell spread in the hydrogel matrix may not be able to faithfully represent disease states. Indeed, spheroids as building blocks could be an alternative and implementable approach.¹⁶³ Swaminathan *et al.* have investigated the bioprinting of pre-formed breast epithelial spheroids by co-culture of endothelial cells with alginate and demonstrated that the printed pre-formed spheroids exhibited high cell viability.¹⁶⁴ A co-culture model of adipose-derived stromal cells and breast cancer cells in a 3D-printed way has



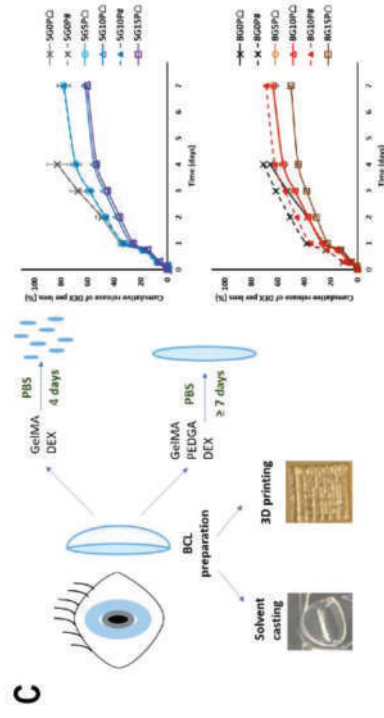
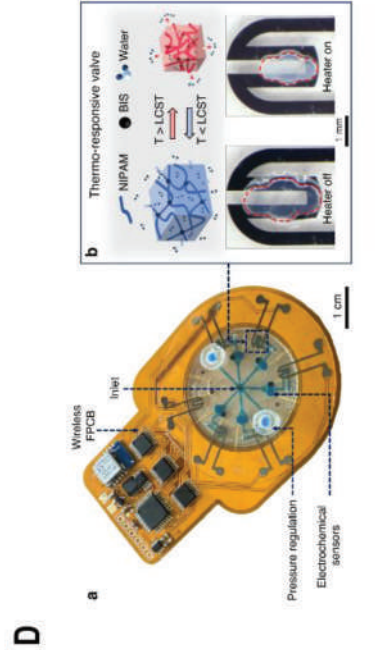
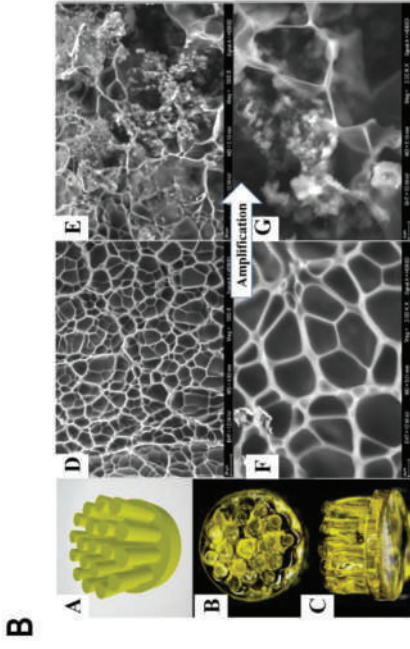
been developed by Horder *et al.*, and the ECM remodeling process can be demonstrated by staining for the major ECM components.¹⁶⁵

In addition to cancer treatment, there is a need for further development of treatment methods for other disease conditions. Multicomponent hydrogels are increasingly used to improve and expand the range of applications, which could improve cell spreading and proliferation, printability, or migration of stratification in combination with innovative approaches, such as 3D printing.¹⁶⁶ For example, a naturally-derived blood vessel network fabricated by printing cell (endothelial cell and fibroblast)-laden decellularized extracellular matrix bioink within a PCL frame was introduced into an airway model to form a vessel-air model, and this model presented respiratory symptoms such as asthmatic airway inflammation in the physiological context (see Figure 8.11A).¹⁶⁷ For physiological units, involving multiple cells and immune responses into disease models is critical. Park *et al.* have developed a 3D adipose tissue model with immune cells, which could form lipid droplets, induce insulin resistance, and allow each cell type to separately grow and differentiate.¹⁶⁸ Lee *et al.* have developed a 3D liver fibrosis model with three liver cell types cultured with gelatin, which could effectively evaluate gene expression, collagen production, apoptosis, and liver function losses in liver fibrosis disease.¹⁶⁹ Zhao *et al.* have developed 3D cervical tumor models which exhibit higher MMP protein expression and higher chemoresistance compared to the conventional 2D planar culture.¹⁷⁰ Other physiological structures, like renal tubules,¹⁷¹ intervertebral disc,¹⁷² neuromuscular junction,¹⁷³ and cardiac tissue,¹⁷⁴ could also be reconstructed through 3D printing of multicomponent hydrogels and could maintain better physiological activity than 2D culture (see Figure 8.11C and D). The results show that 3D printing models could be more representative of *in vivo* tissue and cheaper than testing *in vivo*.

8.4.3 Biosensing and Bioelectronics

Hydrogels are an ideal matrix for many sensing methodologies due to their ability to maximize the interaction between sensors and objects with an

Figure 8.11 Examples of applications in disease modeling and drug testing. (A) Fabrication and structure of vascularized airway-on-a-chip by 3D cell printing, which also includes the microstructure of airway mucosa. Adapted from ref. 167 with permission from IOP Publishing, Copyright 2018. (B) Cellular morphology of the cervical tumor model during eight days of culture. Adapted from ref. 170 with permission from IOP Publishing, Copyright 2014. (C) Schematic illustration of coaxial cell-printing of 3D vascularized renal (top) and fluorescence micrographs of cultured renal tubule and blood vessels (bottom). Adapted from ref. 171 with permission from Elsevier, Copyright 2020. (D) Schematic depicting the fabrication of engineered heart tissue and fluorescence micrographs of actin filaments formed by cardiomyocytes. Adapted from ref. 174 with permission from Elsevier, Copyright 2019.



enhanced capability of changing the functional properties of hydrogels in response to different stimulations.

The most common way to make hydrogel-based sensors is to directly fabricate responsive materials, such as thermo-responsive,¹⁷⁵ pH-responsive,¹⁷⁶ electronic-responsive,¹⁷⁷ and light-sensitive hydrogels. Another common strategy is to add stimuli-responsive entities, such as nanoparticles, functional polymer chains, and DNA, into hydrogels to create inhomogeneous structures. Both approaches highlight the importance of multi-components in hydrogel sensing applications: single-component hydrogels likely fail to satisfy structural support and signal response at the same time. Here, we take electrically conductive hydrogels as an example to show the fabrication method of multicomponent sensing hydrogels, which have been at the frontline of “3D printed biosensors” due to their ability to couple with electronic components and circuits. One method is to directly fabricate conductive polymers into hydrogels, including *in situ*- and post-polymerization of conductive polymers.¹⁷⁸ Another method is adding conductive particles or conductive ionic solution to achieve conductivity.¹⁷⁹

After obtaining the responsive hydrogels, it can step into the process of sensor structure fabrication through 3D printing. Bruen *et al.* have developed sugar-responsive 3D printed scaffolds through co-polymerization of a fluorophore pair with GelMA, which could be used for glucose detection in cell culture¹⁸⁰ (see Figure 8.12A). Apart from chemical elements, living cells could also be involved in creating hydrogel sensors through 3D printing. Jiang *et al.* have built a wheat allergen gliadin sensor by printing a cluster-shaped microvillus structure of the small intestine and immobilizing the rat basophilic leukemia cells on this GelMA-based printed structure. This sensor could detect wheat gliadin covering the range 0.1–0.8 ng mL¹⁸¹ (see Figure 8.12B). However, responsive hydrogels are still isotropic materials, which may have difficulty selectively triggering and conducting specific responses. This challenge highlights the importance of fabrication methods. For example, cross-linking density is the intrinsic parameter for designing performance, which can be varied by adjusting polymer components,

Figure 8.12 Examples of applications in biosensors. (A)–(A) Schematic of generation of BA-GelMA hydrogel scaffolds. (B) Microscopy images of the sensor structure in a buffer. (C) Scanning electron microscopy of the hydrogel scaffold and fluorescence response of the hydrogel scaffolds in 0–100 mM glucose. Adapted from ref. 180 with permission from John Wiley & Sons, Copyright © 2020 Wiley-VCH Verlag GmbH & Co. KGaA, Weinheim. (B) Characterization of the intestinal microvilli and composite hydrogel. Adapted from ref. 181 with permission from Elsevier, Copyright 2021. (C) Schematic diagram of the gelatin-based drug-eluting bandage contact lenses (left) and drug release profiles of contact lenses (right). Adapted from ref. 183 with permission from Elsevier, Copyright 2021. (D) Illustration of a wearable bioanalytical platform. Adapted from ref. 175, <https://doi.org/10.1038/s41467-020-18238-6>, under the terms of the CC BY 4.0 license, <https://creativecommons.org/licenses/by/4.0/>.

and tuning these different parameters modulates the apparent mesh size, mechanical moduli, and permeability in response to different environmental stimuli. Bayles *et al.* have fabricated hydrogel layers with different cross-linking densities by combining advective assembly with 3D printing, which could be used as soft actuators or sensors responding to swelling stimuli.¹⁸²

A promising application of hydrogel surface sensors is contact lenses. Zidan *et al.* prepared drug-loaded GelMA hydrogels with different concentrations of poly(ethylene glycol) diacrylate and fabricated this hydrogel into contact lenses using 3D printing, which could respond to the ocular environment and enable drug release¹⁸³ (see Figure 8.12C). 3D printing of hydrogels is also widely used for mechanical sensors and flexible sensors on biological surfaces. Darabi *et al.* have attained a self-healing and conductive hydrogel, which has pressure and extension sensitive features and could be printed as wearable sensors for respiration and wrist pulse monitoring.¹⁸⁴ Liu *et al.*, Zhu *et al.*, Peng *et al.*, and Wang *et al.* also developed 3D printing patches as skin-inspired sensors for motion, humidity, temperature, and pressure monitoring using multi-component hydrogels^{184,185} (see Figure 8.12D). Another fabrication strategy called *in situ* 3D printing has been developed to make hydrogel sensors on moving freeform surfaces. Zhu *et al.* have directly printed ionic conductive hydrogels on the skin and lung surface with the help of a 3D scanner, which could estimate not only the motion but also the deformation of the target surface as they are thin and deformable.¹⁸⁶

8.4.4 Soft Robotics in Biomedicine

Soft robotics typically make use of flexible substrates to meet the requirement for the softness of the environment or receivers. Compared to hard robotics, soft ones usually rely on material properties for actuation, and their driving methods are more versatile. Moreover, the softness and biocompatibility of many soft robotics make them suitable for a wider application scenario in the biomedical field.

The materials used to construct a soft actuator include flexible fluid, shape-memory polymers, electroactive polymers, and hydrogels. Compared with other materials, hydrogels stand out in biomedicine owing to their good biocompatibility. In addition, the softness of hydrogels allows them to achieve flexible movements. The ability to respond to a wide range of stimuli to achieve large volume changes broadens the range of functions in soft robotics. For example, some dynamic hydrogels have a self-healing property, which could enable soft robotics to regain shape and functionality after large deformations and to be used multiple times.

The responsive nature of soft robotics usually calls for heterogeneity in both their geometry and components, thus leading to a great demand for processing multicomponent hydrogels into complex geometry. The concept of 4D printing has been widely used to develop hydrogel-based soft

actuators. 4D printing adds a dimension of time to 3D printing, where the printed structure changes over time due to external stimuli. In this scenario, different actuation driving methods have been used, and the most widely used one is osmotic actuation. The change of the osmotic pressure subsequently leads to changes in volume and shape. Bakarich *et al.* designed and 3D-printed a temperature-controlled smart valve using an alginate/PNIPAAm-based gel ink (see Figure 8.13A).¹⁸⁷ This material undergoes a reversible volume change near the critical temperature (32–35 °C). This valve reduces the flow rate by 99% when exposed to hot water, while it returns to normal in cold water. Gladman *et al.* designed an ink formulation composed of cellulose fibers embedded in a soft acrylamide matrix (see Figure 8.13B).¹⁸⁸ This ink allows the alignment of the cellulose to be adjusted during the 3D printing process, resulting in a printed structure with

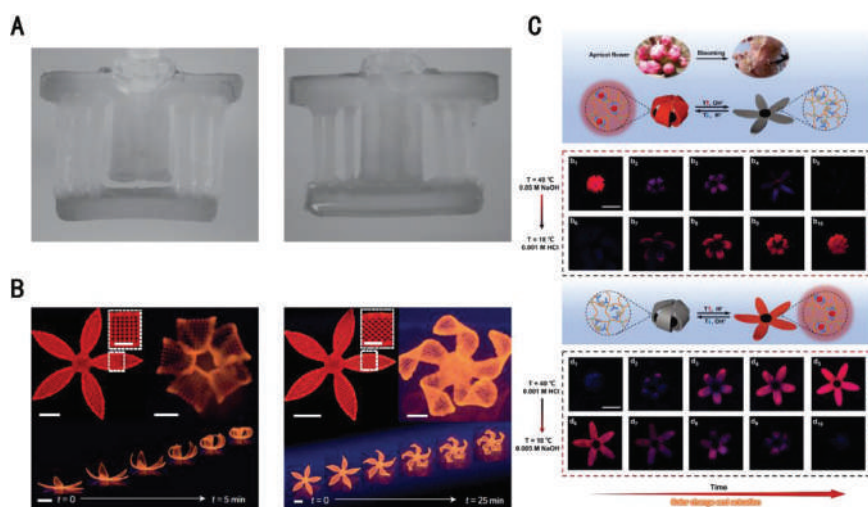


Figure 8.13 Examples of applications in 3D printed hydrogel soft actuators. (A) A temperature-controlled smart valve is fabricated by 3D printing of an alginate/PNIPAAm-based ionic covalent entanglement (ICE) gel ink, showing different deformations at 20 °C (left) and 60 °C (right). Adapted from ref. 187 with permission from John Wiley & Sons, Copyright © 2015 Wiley-VCH Verlag GmbH & Co. KGaA, Weinheim. (B) A swelling-triggered shape-change flower-like structure is fabricated *via* extrusion-based 3D printing of ink composed of cellulose fibers embedded in a soft acrylamide matrix. The flowers composed of 90°/0° and -45°/45° bilayers oriented with respect to the long axis of each petal could change their shape accordingly with time-lapse sequences. Adapted from ref. 188 with permission from Springer Nature, Copyright 2016. (C) An artificial apricot flower based on a shape-memory composite polymer capable of synergistic color-changing and shape-deformation in response to the subtle interplay between temperature and acidity/alkalinity changes. Adapted from ref. 189 with permission from John Wiley & Sons, Copyright © 2019 Wiley-VCH Verlag GmbH & Co. KGaA, Weinheim. Scale bars: $B = 5$ mm, $B(\text{inset}) = 2.5$ mm, $C = 10$ mm.

anisotropic swelling behavior. In another example, Wei *et al.* designed a multicomponent hydrogel material that can change color depending on the environmental pH-value and metal ions (see Figure 8.13C).¹⁸⁹ They used it to 3D-print hydrogel apricot flowers, which can change shape and color simultaneously. Cell-driven actuation is another interesting method, where cell traction force is usually applied to drive the deformation of soft substrates. It has the advantage of exploiting the self-healing properties and adaptability of hydrogels. The challenge lies in the composition of the suitable hydrogel and macroscopic movement due to the limited force generated by cells. Recently, Lee *et al.* developed an autonomously swimming biohybrid fish equipped with an antagonistic muscular bilayer.¹⁹⁰ The mechanical coupling between the two layers of cardiomyocytes enables the contraction of one side to be translated directly into an axial stretch of the opposite side, leading to antagonistic muscle excitation and contraction. In the experiment, this fish was able to swim continuously for 108 days. Pneumatic, hydraulic, magnetic, and acoustic actuation are used in soft actuators as well. These methods do not rely on the swelling effect of hydrogels but tend to have higher drive efficiency.

Soft robotics based on 3D printed multicomponent hydrogels are still facing many challenges. The mechanical strength of the hydrogel limits its movement ability. More efficient and multi-factor actuation methods also need to be developed. In terms of performance, more precise control, greater stability, and self-recovery are all desired. On the manufacturing side, advanced 3D printing processes that allow for the fabrication of more sophisticated structures could also advance soft robotics. Considering the fact that current studies are mostly limited to the laboratory, efforts are also needed toward translational use in biomedicine.

8.4.5 Other Biomedical Devices

3D printing can benefit the field of biomedical devices in a customized manner. Apart from the advances listed above, here we highlight the additional application areas of 3D printed biomedical devices based on multicomponent hydrogels. A straightforward use of 3D printed hydrogel constructs is to serve as high-fidelity training or education platforms owing to the fabrication capability of 3D printing and the high mechanical similarity of the hydrogel to human tissues. These training platforms, including the middle cerebral artery model, partial nephrectomy, coronary artery bypass, cervical laminectomy, *etc.*, not only show high anatomical accuracy and realistic tissue properties but also exhibit lower cost and easier accessibility than traditional training platforms.¹⁹¹

3D printing of microrobots is also noteworthy, which aims to develop micromachines that are physically and/or chemically propelled and programmed to implement miscellaneous complex missions within the human body or in the natural environment.¹⁹² Photopolymerizable hydrogels are widely used for the fabrication of microrobots, such as GelMA, MeHA, and

Table 8.3 Biomedical applications of 3D printed multicomponent hydrogels.

Category	Applications	Main feature(s)	Ref.
Tissue engineering and regenerative medicine	Hard mandibular bone fragment	<ul style="list-style-type: none"> • Multicomponent hydrogel of gelatin, fibrinogen, HA, glycerol and stem cells 	21
	Multilayer osteochondral alternative tissue	<ul style="list-style-type: none"> • Divided into mineralized biomaterial phases, hydrogels loaded with human chondrocytes and hydrogels loaded with mesenchymal stromal cells • Considerable cell viability and metabolic activity, and good printability 	149
	Islet cell and diabetes model	<ul style="list-style-type: none"> • Preserve islet cell morphology within the hydrogel for seven days 	151
	Spinal neural structure	<ul style="list-style-type: none"> • Made of a combination of Matrigel, gelatin/fibrin, and GelMA and a cell mixture of oligodendrocyte progenitor cells and derived spinal neural progenitor cells 	159
Disease modeling and drug testing	Spheroid bioprinting breast cancer models	<ul style="list-style-type: none"> • Developing personalized breast cancer therapy and drug screening 	155
	Tumor bonelike microenvironment	<ul style="list-style-type: none"> • Photopolymerization-based 3D printing • Study the behavior of cancer invasion in microstructures 	159
	Pulmonary artery models	<ul style="list-style-type: none"> • Vascularized airway-on-a-chip • Microstructure of airway mucosa 	167
	3D liver fibrosis models	<ul style="list-style-type: none"> • Involving three liver cell types • Effectively evaluate gene expression and liver function losses 	169
Biosensing and bioelectronics	The GelMA scaffolds used to detect glucose	<ul style="list-style-type: none"> • Co-polymerize the fluorophore pair 	180
	The wheat allergen gliadin sensor	<ul style="list-style-type: none"> • Involving living microvillus cells as sensors 	181
	Wearable sensors	<ul style="list-style-type: none"> • Skin-inspired sensor for motion, humidity, temperature, and pressure monitoring 	175
	Contact lenses	<ul style="list-style-type: none"> • Could respond to the ocular environment and enable drug release 	183
Soft robotics	Temperature-controlled smart valve	<ul style="list-style-type: none"> • Reversible volume change when exposed to different temperatures 	187
	Swimming biohybrid fish	<ul style="list-style-type: none"> • Be able to swim continuously for 108 days 	190

PEG acrylates. For example, Zhu *et al.* have developed a 3D microscale continuous optical printing method to engineer functionalized microrobots. By constructing PEGDA-based composite hydrogels with functional nanoparticles, the microrobots could be fabricated with magnetic Fe_3O_4 nanoparticles at the head and catalytic Pt nanoparticles at the tail, which can control the swimming direction and speed of the microrobots.¹⁹³ Also, Park *et al.* have fabricated a magnetically driven porous degradable microrobot which consists of a PEGDA and pentaerythritol triacrylate matrix containing magnetite nanoparticles and the anticancer drug 5-fluorouracil. The microrobot could also be actuated by magnetic fields, thanks to magnetite nanoparticles, and the porous structure facilitates the ultrasound-induced drug release, which can be selected on command from three different modes by different ultrasound exposure conditions.¹⁹⁴

Hydrogels could also print into origami structures to evolve in structure response to their environment, which could be optimized for different purposes. It takes advantage of the responsive properties of hydrogels, which combine the benefit of planar fabrication methods with the complexity achievable through folding. For example, Baker *et al.* have fabricated origami structures formed by a hydrogel core trilayer with a polyurethane elastomer skin bilayer, which causes shape-change during submersion in water and returns to the configuration after dehydration.¹⁹⁵ Other elaborate and complex origami structures, such as helices and chains, can be fabricated by 3D printing, which can complete reversible structure changes in response to factors such as temperature and humidity, thanks to the incorporation of multiple components into hydrogels.¹⁹⁵ These 3D-printed origami structures show promise in fabricating foldable devices, such as foldable robots and electronics (see Table 8.3).

8.5 Concluding Remarks

The extrusion-based approach could readily process multi-materials simultaneously *via* the use of multi-nozzles or other versatile multi-input strategies to yield heterogeneity, which has been systemically reviewed in this chapter. Vat photopolymerization-based 3D printing is another attractive approach and has been seen with exciting progress, such as volumetric 3D printing in seconds and high-resolution printing of complex vascular networks in hydrogels. Despite the efforts in processing multiple inks into one construct *via* the switch of vats or *in situ* refilling approaches, the fabrication of multicomponent constructs remains an enduring challenge due to the nature of vat-polymerization. Droplet jetting-based 3D printing exhibits the advantages of high speed and resolution but is usually limited to low-viscosity inks, which makes it challenging for 3D construction.

Regarding the multicomponent hydrogels being used in 3D printing, we have made a careful classification of the formulation types and overviewed the most recent progress accordingly. The conventional miscible systems would usually yield enhanced mechanical properties (*e.g.*, injectability and

high stiffness) *via* the use of various materials preparation strategies (*e.g.*, interpenetrating networks and supramolecular chemistry). Recently, immiscible systems have emerged as an important approach for engineering heterogeneous hydrogel structures. Bulk hydrogels can be supplemented with multiscale components, ranging from nanocomposites to microphase, to yield specific properties, such as conductivity, microporosity, bio-functionality, and 3D printability. One of the most exciting and straightforward applications of these 3D printed multicomponent hydrogels is engineering bio-functional tissues or organs for regenerative medicine. This leads to a more focused area termed 3D bioprinting, which usually introduces living cells to the fabrication process and generates cellularized products that serve as tissue implants. Beyond regenerative medicine, bioprinted products can also serve as disease and drug testing models for pathological and pharmaceutical applications. Notably, bioprinted drug testing models attracted much attention owing to their excellent reproducibility and biological relevance compared with the traditional 2D cell culture models. Apart from these areas, the 3D printing of multicomponent hydrogels has also shown great potential in biosensing, bioelectronics, soft robotics, and other biomedical applications.

Abbreviations

ITOP	Integrated tissue–organ printer
PCL	Polycaprolactone
LIFT	Laser-induced forward transfer
AJP	Aerosol jet printing
EJP	Electrohydrodynamic jet printing
SLA	Stereolithography
DLP	Digital light processing
CLIP	Continuous liquid interface production
TPP	Two-photon polymerization
ECM	Extracellular matrix
HAMA	Methacrylated hyaluronic acid
PEDOT	Poly(3,4-ethylenedioxythiophene)
PEG	Polyethylene glycol
PEGX	PEG crosslinkers
IPN	Interpenetrating network
DN	Double-network
SF	Silk fibroin
PVP	Polyvinylpyrrolidone
DIW	Direct ink writing
NHA	Nano-hydroxyapatite
HA	Hyaluronic acid
Ad	Adamantane
CD	β -Cyclodextrin
ATPS	Aqueous two-phase system

PEO	Polyethylene oxide
DEX	Dextran
CNTs	Carbon nanotubes
ADA	Alginate dialdehyde
GEL	Gelatin
OC	Osteochondral
GNR	Gold nanorod
BNC	Bacterial nanocellulose hydrogels
CNC	Cellulose nanocrystals
CNF	Cellulose nanofibers
HMPs	Hydrogel microparticles
GO	Graphene oxide
NSC	Neural stem cells
BG	Bioactive glass
ICE	Ionic covalent entanglement

Acknowledgements

The authors acknowledge the financial support from the National Natural Science Foundation of China (No. 52105306), Faculty Start-up Funding (012-53330200421), and the Student Research Training program (SRT 2121T0134) of Tsinghua University.

References

1. Z. Fu, L. Ouyang, R. Xu, Y. Yang and W. Sun, *Mater. Today*, 2022, **52**, 112–132.
2. L. Ouyang, *Trends Biotechnol.*, 2022, **40**, 891–902.
3. C. W. Hull, *US Pat. Appl.*, 638905, 1984.
4. W. Sun and J. Nam, *US Pat. Appl.*, 540968, 2005.
5. H. Kodama, *Rev. Sci. Instrum.*, 1981, **52**, 1770–1773.
6. S. Derakhshanfar, R. Mbeleck, K. Xu, X. Zhang, W. Zhong and M. Xing, *Bioact. Mater.*, 2018, **3**, 144–156.
7. A. Lee, A. R. Hudson, D. J. Shiwerski, J. W. Tashman, T. J. Hinton, S. Yerneni, J. M. Bliley, P. G. Campbell and A. W. Feinberg, *Science*, 2019, **365**, 482–487.
8. S. V. Murphy and A. Atala, *Nat. Biotechnol.*, 2014, **32**, 773–785.
9. D. Kang, G. Hong, S. An, I. Jang, W.-S. Yun, J.-H. Shim and S. Jin, *Small*, 2020, **16**, 1905505.
10. H. Gudapati, M. Dey and I. Ozbolat, *Biomaterials*, 2016, **102**, 20–42.
11. J. R. Tumbleston, D. Shirvanyants, N. Ermoshkin, R. Januszewicz, A. R. Johnson, D. Kelly, K. Chen, R. Pinschmidt, J. P. Rolland, A. Ermoshkin, E. T. Samulski and J. M. DeSimone, *Science*, 2015, **347**, 1349–1352.
12. K. K. B. Hon, L. Li and I. M. Hutchings, *CIRP Ann.*, 2008, **57**, 601–620.

13. Y.-G. Park, I. Yun, W. G. Chung, W. Park, D. H. Lee and J.-U. Park, *Adv. Sci.*, 2022, **9**, 2104623.
14. O. Jeon, Y. B. Lee, H. Jeong, S. J. Lee, D. Wells and E. Alsberg, *Mater. Horiz.*, 2019, **6**, 1625–1631.
15. W. L. Ng, J. M. Lee, W. Y. Yeong and M. Win Naing, *Biomater. Sci.*, 2017, **5**, 632–647.
16. Z. Wang, X. Jin, Z. Tian, F. Menard, J. F. Holzman and K. Kim, *Adv. Healthcare Mater.*, 2018, **7**, 1701249.
17. F. Zhang, L. Zhu, Z. Li, S. Wang, J. Shi, W. Tang, N. Li and J. Yang, *Addit. Manuf.*, 2021, **48**, 102423.
18. J.-F. Xing, M.-L. Zheng and X.-M. Duan, *Chem. Soc. Rev.*, 2015, **44**, 5031–5039.
19. W. L. Ng, J. M. Lee, M. Zhou, Y.-W. Chen, K.-X. A. Lee, W. Y. Yeong and Y.-F. Shen, *Biofabrication*, 2020, **12**, 022001.
20. M. Regehly, Y. Garmshausen, M. Reuter, N. F. König, E. Israel, D. P. Kelly, C.-Y. Chou, K. Koch, B. Asfari and S. Hecht, *Nature*, 2020, **588**, 620–624.
21. H. W. Kang, S. J. Lee, I. K. Ko, C. Kengla, J. J. Yoo and A. Atala, *Nat. Biotechnol.*, 2016, **34**, 312–319.
22. W. J. Liu, Y. S. Zhang, M. A. Heinrich, F. De Ferrari, H. L. Jang, S. M. Bakht, M. M. Alvarez, J. Z. Yang, Y. C. Li, G. Trujillo-de Santiago, A. K. Miri, K. Zhu, P. Khoshakhlagh, G. Prakash, H. Cheng, X. F. Guan, Z. Zhong, J. Ju, G. H. Zhu, X. Y. Jin, S. R. Shin, M. R. Dokmeci and A. Khademhosseini, *Adv. Mater.*, 2017, **29**, 1604630.
23. M. A. Skylar-Scott, J. Mueller, C. W. Visser and J. A. Lewis, *Nature*, 2019, **575**, 330–335.
24. L. Shao, Q. Gao, C. Xie, J. Fu, M. Xiang and Y. He, *Biofabrication*, 2020, **12**, 035014.
25. D. Kang, G. Ahn, D. Kim, H.-W. Kang, S. Yun, W.-S. Yun, J.-H. Shim and S. Jin, *Biofabrication*, 2018, **10**, 035008.
26. N. Noor, A. Shapira, R. Edri, I. Gal, L. Wertheim and T. Dvir, *Adv. Sci.*, 2019, **6**, 1900344.
27. G. Lee, S. J. Kim, H. Chun and J.-K. Park, *Biofabrication*, 2021, **13**, 045027.
28. J. He, J. Shao, X. Li, Q. Huang and T. Xu, *Bioprinting*, 2018, **11**, e00036.
29. M. Xie, Q. Gao, J. Qiu, J. Fu, Z. Chen and Y. He, *Biomater. Sci.*, 2020, **8**, 109–117.
30. J. Zhu, W. Huang, Q. Zhang, S. Ling, Y. Chen and D. L. Kaplan, *Materials*, 2016, **9**, 221.
31. L. Ouyang, C. B. Highley, W. Sun and J. A. Burdick, *Adv. Mater.*, 2017, **29**, 1604983.
32. J. T. Muth, D. M. Vogt, R. L. Truby, Y. Menguc, D. B. Kolesky, R. J. Wood and J. A. Lewis, *Adv. Mater.*, 2014, **26**, 6307–6312.
33. T. Bhattacharjee, S. M. Zehnder, K. G. Rowe, S. Jain, R. M. Nixon, W. G. Sawyer and T. E. Angelini, *Sci. Adv.*, 2015, **1**, e1500655.

34. A. McCormack, C. B. Highley, N. R. Leslie and F. P. W. Melchels, *Trends Biotechnol.*, 2020, **38**, 584–593.
35. A. Soleimani-Gorgani, in *Printing on Polymers*, ed. J. Izdebska and S. Thomas, William Andrew Publishing, 2016, pp. 231–246.
36. J. A. Park, S. Yoon, J. Kwon, H. Now, Y. K. Kim, W. J. Kim, J. Y. Yoo and S. Jung, *Sci. Rep.*, 2017, **7**, 14610.
37. K. Christensen, C. Xu, W. Chai, Z. Zhang, J. Fu and Y. Huang, *Biotechnol. Bioeng.*, 2015, **112**, 1047–1055.
38. A. Faulkner-Jones, C. Fyfe, D. J. Cornelissen, J. Gardner, J. King, A. Courtney and W. Shu, *Biofabrication*, 2015, **7**, 044102.
39. K. Shigeta, Y. He, E. Sutanto, S. Kang, A.-P. Le, R. G. Nuzzo, A. G. Alleyne, P. M. Ferreira, Y. Lu and J. A. Rogers, *Anal. Chem.*, 2012, **84**, 10012–10018.
40. L. Koch, A. Deiwick, S. Schlie, S. Michael, M. Gruene, V. Coger, D. Zychlinski, A. Schambach, K. Reimers, P. M. Vogt and B. Chichkov, *Biotechnol. Bioeng.*, 2012, **109**, 1855–1863.
41. R. Xiong, Z. Zhang, W. Chai, Y. Huang and D. B. Chrisey, *Biofabrication*, 2015, **7**, 045011.
42. T. Rahman, L. Renaud, D. Heo, M. Renn and R. Panat, *J. Micromech. Microeng.*, 2015, **25**, 107002.
43. X. Li, B. Liu, B. Pei, J. Chen, D. Zhou, J. Peng, X. Zhang, W. Jia and T. Xu, *Chem. Rev.*, 2020, **120**, 10596–10636.
44. Y. Sun, X. Zhou and Y. Yu, *Lab Chip*, 2014, **14**, 3603–3610.
45. B. V. Antohe and D. B. Wallace, *Msec 2008: Proceedings of the Asme International Manufacturing Science and Engineering Conference*, 2008, vol. 2, pp. 525–533.
46. J. Sun, J. H. Ng, Y. H. Fuh, Y. S. Wong, H. T. Loh and Q. Xu, *Microsyst. Technol.*, 2009, **15**, 1437–1448.
47. A. Faulkner-Jones, S. Greenhough, J. A. King, J. Gardner, A. Courtney and W. Shu, *Biofabrication*, 2013, **5**, 015013.
48. A. Blaeser, D. F. Duarte Campos, U. Puster, W. Richtering, M. M. Stevens and H. Fischer, *Adv. Healthcare Mater.*, 2016, **5**, 326–333.
49. A. Jaworek and A. Krupa, *J. Aerosol Sci.*, 1999, **30**, 873–893.
50. N. Mkhize and H. Bhaskaran, *Small Sci.*, 2022, **2**, 2100073.
51. M. Mao, H. Liang, J. He, A. Kasimu, Y. Zhang, L. Wang, X. Li and D. Li, *Int. J. Bioprint.*, 2021, **7**, 86–96.
52. M. Duocastella, J. M. Fernández-Pradas, J. L. Morenza and P. Serra, *J. Appl. Phys.*, 2009, **106**, 084907.
53. T. Smausz, B. Hopp, G. Kecskemeti and Z. Bor, *Appl. Surf. Sci.*, 2006, **252**, 4738–4742.
54. V. I. Yusupov, V. S. Zhigar'kov, E. S. Churbanova, E. A. Chutko, S. A. Evlashin, M. V. Gorlenko, V. S. Cheptsov, N. V. Minaev and V. N. Bagratashvili, *Quantum Electron.*, 2017, **47**, 1158–1165.
55. D. M. Kingsley, A. D. Dias, D. B. Chrisey and D. T. Corr, *Biofabrication*, 2013, **5**, 045006.

56. B. Guillotin, A. Souquet, S. Catros, M. Duocastella, B. Pippenger, S. Bellance, R. Bareille, M. Remy, L. Bordenave, J. Amedee and F. Guillemot, *Biomaterials*, 2010, **31**, 7250–7256.
57. T. Xu, C. Baicu, M. Aho, M. Zile and T. Boland, *Biofabrication*, 2009, **1**, 035001.
58. U. Demirci and G. Montesano, *Lab Chip*, 2007, **7**, 1139–1145.
59. Z. Gong, L. Huang, X. Tang, K. Chen, Z. Wu, L. Zhang, Y. Sun, Y. Xia, H. Chen, Y. Wei, F. Wang and S. Guo, *Adv. Healthcare Mater.*, 2021, **10**, 2101312.
60. D. Zhou, J. Chen, B. Liu, X. Zhang, X. Li and T. Xu, *Bioprinting*, 2019, **16**, e00060.
61. Y. Fang, J. P. Frampton, S. Raghavan, R. Sabahi-Kaviani, G. Luker, C. X. Deng and S. Takayama, *Tissue Eng., Part C*, 2012, **18**, 647–657.
62. F. Guo, Z. M. Mao, Y. C. Chen, Z. W. Xie, J. P. Lata, P. Li, L. Q. Ren, J. Y. Liu, J. Yang, M. Dao, S. Suresh and T. J. Huang, *Proc. Natl. Acad. Sci. U. S. A.*, 2016, **113**, 1522–1527.
63. J. M. Shapiro, B. W. Drinkwater, A. W. Perriman and M. Fraser, *Adv. Mater. Technol.*, 2021, **6**, 2000689.
64. D. Foresti, K. T. Kroll, R. Amisshah, F. Sillani, K. A. Homan, D. Poulikakos and J. A. Lewis, *Sci. Adv.*, 2018, **4**, 9.
65. J. M. Hoey, A. Lutfurakhmanov, D. L. Schulz and I. S. Akhatov, *J. Nanotechnol.*, 2012, 324380.
66. G. L. Goh, S. Agarwala, Y. J. Tan and W. Y. Yeong, *Sens. Actuators, B*, 2018, **260**, 227–235.
67. C. Cooper and B. Hughes, *Aerosol jet printing of electronics: an enabling technology for wearable devices*, 2020.
68. N. J. Wilkinson, M. A. A. Smith, R. W. Kay and R. A. Harris, *Int. J. Adv. Manuf. Technol.*, 2019, **105**, 4599–4619.
69. J. H. Cho, J. Lee, Y. Xia, B. Kim, Y. He, M. J. Renn, T. P. Lodge and C. D. Frisbie, *Nat. Mater.*, 2008, **7**, 900–906.
70. M. S. Saleh, C. Hu and R. Panat, *Sci. Adv.*, 2017, **3**, e1601986.
71. J. G. Tait, E. Witkowska, M. Hirade, T.-H. Ke, P. E. Malinowski, S. Steudel, C. Adachi and P. Heremans, *Org. Electron.*, 2015, **22**, 40–43.
72. G. I. Peterson, J. J. Schwartz, D. Zhang, B. M. Weiss, M. A. Ganter, D. W. Storti and A. J. Boydston, *ACS Appl. Mater. Interfaces*, 2016, **8**, 29037–29043.
73. Z. H. Zhang, N. Corrigan, A. Bagheri, J. Y. Jin and C. Boyer, *Angew. Chem., Int. Ed.*, 2019, **58**, 17954–17963.
74. D. Han, C. Yang, N. X. Fang and H. Lee, *Addit. Manuf.*, 2019, **27**, 606–615.
75. F. Mayer, S. Richter, J. Westhauser, E. Blasco, C. Barner-Kowollik and M. Wegener, *Sci. Adv.*, 2019, **5**, eaau9160.
76. X. Mu, T. Bertron, C. Dunn, H. Qiao, J. Wu, Z. Zhao, C. Saldana and H. J. Qi, *Mater. Horiz.*, 2017, **4**, 442–449.
77. Q. Mu, L. Wang, C. K. Dunn, X. Kuang, F. Duan, Z. Zhang, H. J. Qi and T. Wang, *Addit. Manuf.*, 2017, **18**, 74–83.

78. S.-R. Hwang and M.-S. Park, *Appl. Sci.*, 2021, **11**, 8545.
79. B. E. Kelly, I. Bhattacharya, H. Heidari, M. Shusteff, C. M. Spadaccini and H. K. Taylor, *Science*, 2019, **363**, 1075–1079.
80. N. D. Dolinski, Z. A. Page, E. B. Callaway, F. Eisenreich, R. V. Garcia, R. Chavez, D. P. Bothman, S. Hecht, F. W. Zok and C. J. Hawker, *Adv. Mater.*, 2018, **30**, 1800364.
81. J. J. Schwartz and A. J. Boydston, *Nat. Commun.*, 2019, **10**, 791.
82. N. D. Dolinski, E. B. Callaway, C. S. Sample, L. F. Gockowski, R. Chavez, Z. A. Page, F. Eisenreich, S. Hecht, M. T. Valentine, F. W. Zok and C. J. Hawker, *ACS Appl. Mater. Interfaces*, 2021, **13**, 22065–22072.
83. J. Wu, Z. Zhao, X. Kuang, C. M. Hamel, D. Fang and H. J. Qi, *Multifunct. Mater.*, 2018, **1**, 015002.
84. C. W. Hull, *US Pat.*, 638905, 1984.
85. S. C. Ligon, R. Liska, J. Stampfl, M. Gurr and R. Muelhaupt, *Chem. Rev.*, 2017, **117**, 10212–10290.
86. P. Robles-Martinez, X. Xu, S. J. Trenfield, A. Awad, A. Goyanes, R. Telford, A. W. Basit and S. Gaisford, *Pharmaceutics*, 2019, **11**, 274.
87. J. M. Lee, S. L. Sing, M. Zhou and W. Y. Yeong, *Int. J. Bioprint.*, 2018, **4**, 151.
88. M. Farsari, M. Vamvakaki and B. N. Chichkov, *J. Opt.*, 2010, **12**, 124001.
89. M. Rumi and J. W. Perry, *Adv. Opt. Photonics*, 2010, **2**, 451–518.
90. D. Jin, Q. Chen, T.-Y. Huang, J. Huang, L. Zhang and H. Duan, *Mater. Today*, 2020, **32**, 19–25.
91. D. Loterie, P. Delrot and C. Moser, *Volumetric 3D printing of elastomers by tomographic back-projections*, 2018.
92. D. Loterie, P. Delrot and C. Moser, *Nat. Commun.*, 2020, **11**, 852.
93. Y. W. Wang, W. J. Bao, F. Wang, H. Y. Zhang, Z. H. Wang and Y. H. Wang, *J. Micromech. Microeng.*, 2020, **30**, 035002.
94. J. M. Grolman, D. Zhang, A. M. Smith, J. S. Moore and K. A. Kilian, *Adv. Mater.*, 2015, **27**, 5512–5517.
95. J. Yin, M. Yan, Y. Wang, J. Fu and H. Suo, *ACS Appl. Mater. Interfaces*, 2018, **10**, 6849–6857.
96. C.-T. Hsieh and S.-h. Hsu, *ACS Appl. Mater. Interfaces*, 2019, **11**, 32746–32757.
97. B. Duan, E. Kapetanovic, L. A. Hockaday and J. T. Butcher, *Acta Biomater.*, 2014, **10**, 1836–1846.
98. A. L. Rutz, K. E. Hyland, A. E. Jakus, W. R. Burghardt and R. N. Shah, *Adv. Mater.*, 2015, **27**, 1607–1614.
99. C. Colosi, S. R. Shin, V. Manoharan, S. Massa, M. Costantini, A. Barbetta, M. R. Dokmeci, M. Dentini and A. Khademhosseini, *Adv. Mater.*, 2016, **28**, 677–684.
100. S. Hong, D. Sycks, H. F. Chan, S. Lin, G. P. Lopez, F. Guilak, K. W. Leong and X. Zhao, *Adv. Mater.*, 2015, **27**, 4035–4040.
101. Z. Wen, F. Jiang, F. Wu, Z. Yin, K. Kaur, J. Chakraborty, S. Ghosh and S. Lu, *Materialia*, 2020, **9**, 100525.

102. C. B. Highley, C. B. Rodell and J. A. Burdick, *Adv. Mater.*, 2015, **27**, 5075–5079.
103. G.-L. Ying, N. Jiang, S. Mahar, Y.-X. Yin, R.-R. Chai, X. Cao, J.-Z. Yang, A. K. Miri, S. Hassan and Y. S. Zhang, *Adv. Mater.*, 2018, **30**, 1805460.
104. J. R. Xavier, T. Thakur, P. Desai, M. K. Jaiswal, N. Sears, E. Cosgriff-Hernandez, R. Kaunas and A. K. Gaharwar, *ACS Nano*, 2015, **9**, 3109–3118.
105. G. M. Cunniffe, T. Gonzalez-Fernandez, A. Daly, B. N. Sathy, O. Jeon, E. Alsberg and D. J. Kelly, *Tissue Eng., Part A*, 2017, **23**, 891–900.
106. K. Zhu, S. R. Shin, T. van Kempen, Y.-C. Li, V. Ponraj, A. Nasajpour, S. Mandla, N. Hu, X. Liu, J. Leijten, Y.-D. Lin, M. A. Hussain, Y. S. Zhang, A. Tamayol and A. Khademhosseini, *Adv. Funct. Mater.*, 2017, **27**, 1605352.
107. L. Ouyang, J. P. Wojciechowski, J. Tang, Y. Guo and M. M. Stevens, *Adv. Healthcare Mater.*, 2022, **11**, 2200027.
108. S.-J. Lee, W. Zhu, M. Nowicki, G. Lee, D. N. Heo, J. Kim, Y. Y. Zuo and L. G. Zhang, *J. Neural Eng.*, 2018, **15**, 016018.
109. B. Sarker, W. Li, K. Zheng, R. Detsch and A. R. Boccaccini, *ACS Biomater. Sci. Eng.*, 2016, **2**, 2240–2254.
110. L. Ouyang, R. Yao, X. Chen, J. Na and W. Sun, *Biofabrication*, 2015, **7**, 015010.
111. L. Ouyang, R. Yao, S. Mao, X. Chen, J. Na and W. Sun, *Biofabrication*, 2015, **7**, 044101.
112. M. C. Gómez-Guillén, B. Giménez, M. E. López-Caballero and M. P. Montero, *Food Hydrocolloids*, 2011, **25**, 1813–1827.
113. A. Duconseille, T. Astruc, N. Quintana, F. Meersman and V. Sante-Lhoutellier, *Food Hydrocolloids*, 2015, **43**, 360–376.
114. L. Ouyang, J. P. K. Armstrong, Y. Lin, J. P. Wojciechowski, C. Lee-Reeves, D. Hachim, K. Zhou, J. A. Burdick and M. M. Stevens, *Sci. Adv.*, 2020, **6**, eabc5529.
115. A. R. Spencer, E. S. Sani, J. R. Soucy, C. C. Corbet, A. Primbetova, R. A. Koppes and N. Annabi, *ACS Appl. Mater. Interfaces*, 2019, **11**, 30518–30533.
116. J. P. Gong, Y. Katsuyama, T. Kurokawa and Y. Osada, *Adv. Mater.*, 2003, **15**, 1155–1158.
117. J.-Y. Sun, X. Zhao, W. R. K. Illeperuma, O. Chaudhuri, K. H. Oh, D. J. Mooney, J. J. Vlassak and Z. Suo, *Nature*, 2012, **489**, 133–136.
118. E. C. C. Stanford, *Sci. Am.*, 1883, **16**, 6323–6324.
119. X. Yang, Z. Lu, H. Wu, W. Li, L. Zheng and J. Zhao, *Mater. Sci. Eng., C*, 2018, **83**, 195–201.
120. Y. Luo, G. Luo, M. Gelinsky, P. Huang and C. Ruan, *Mater. Lett.*, 2017, **189**, 295–298.
121. S. Midha, S. Murab and S. Ghosh, *Biomaterials*, 2016, **97**, 133–153.
122. Q. Wang, G. Han, S. Yan and Q. Zhang, *Materials*, 2019, **12**, 504.
123. H. Maleki, M.-A. Shahbazi, S. Montes, S. H. Hosseini, M. R. Eskandari, S. Zaunschirm, T. Verwanger, S. Mathur, B. Milow, B. Krammer and N. Huesing, *ACS Appl. Mater. Interfaces*, 2019, **11**, 17256–17269.

124. J. Radhakrishnan, A. Subramanian, U. M. Krishnan and S. Sethuraman, *Biomacromolecules*, 2017, **18**, 1–26.
125. E. A. Appel, J. del Barrio, X. J. Loh and O. A. Scherman, *Chem. Soc. Rev.*, 2012, **41**, 6195–6214.
126. M. J. Webber, E. A. Appel, E. W. Meijer and R. Langer, *Nat. Mater.*, 2016, **15**, 13–26.
127. L. Li, Q. Lin, M. Tang, A. J. E. Duncan and C. Ke, *Chem. – Eur. J.*, 2019, **25**, 10768–10781.
128. C. B. Rodell, A. L. Kaminski and J. A. Burdick, *Biomacromolecules*, 2013, **14**, 4125–4134.
129. T. J. Peters, *Cell Biochem. Funct.*, 1987, **5**, 233–234.
130. R. Hatti-Kaul, *Aqueous two-phase systems: methods and protocols*, Springer Science & Business Media, 2000.
131. H. Tavana and S. Takayama, *Biomicrofluidics*, 2011, **5**, 13404.
132. H. Cabezas, *J. Chromatogr. B: Biomed. Sci. Appl.*, 1996, **680**, 3–30.
133. E. Atefi, R. Joshi, J. A. Mann and H. Tavana, *ACS Appl. Mater. Interfaces*, 2015, **7**, 21305–21314.
134. R. Joshi, B. Fuller, B. Mosadegh and H. Tavana, *J. Tissue Eng. Regener. Med.*, 2018, **12**, 2041–2054.
135. I. Poudel, J. Y. Lim and D. E Menter, *Biomed. Eng. Lett.*, 2012, **2**, 38–45.
136. H. Tavana, B. Mosadegh and S. Takayama, *Adv. Mater.*, 2010, **22**, 2628–2631.
137. G. Luo, Y. Yu, Y. Yuan, X. Chen, Z. Liu and T. Kong, *Adv. Mater.*, 2019, **31**, 1904631.
138. H. Zhang, H. Huang, G. Hao, Y. Zhang, H. Ding, Z. Fan and L. Sun, *Adv. Funct. Mater.*, 2021, **31**, 2006697.
139. N. Annabi, S. R. Shin, A. Tamayol, M. Miscuglio, M. A. Bakooshli, A. Assmann, P. Mostafalu, J.-Y. Sun, S. Mithieux, L. Cheung, X. Tang, A. S. Weiss and A. Khademhosseini, *Adv. Mater.*, 2016, **28**, 40–49.
140. M. Ojansivu, A. Rashad, A. Ahlinder, J. Massera, A. Mishra, K. Syverud, A. Finne-Wistrand, S. Miettinen and K. Mustafa, *Biofabrication*, 2019, **11**, 035010.
141. H. Zhu, M. Monavari, K. Zheng, T. Distler, L. Ouyang, S. Heid, Z. Jin, J. He, D. Li and A. R. Boccaccini, *Small*, 2022, **18**, 2104996.
142. S. Xin, K. A. Deo, J. Dai, N. K. R. Pandian, D. Chimene, R. M. Moebius, A. Jain, A. Han, A. K. Gaharwar and D. L. Alge, *Sci. Adv.*, 2021, **7**, eabk3087.
143. Q. Feng, D. Li, Q. Li, H. Li, Z. Wang, S. Zhu, Z. Lin, X. Cao and H. Dong, *ACS Appl. Mater. Interfaces*, 2022, **14**, 15653–15666.
144. S. H. Kim, H. Hong, O. Ajiteru, M. T. Sultan, Y. J. Lee, J. S. Lee, O. J. Lee, H. Lee, H. S. Park, K. Y. Choi, J. S. Lee, H. W. Ju, I.-S. Hong and C. H. Park, *Nat. Protoc.*, 2021, **16**, 5484–5532.
145. J. Hou, X. Ren, S. Guan, L. Duan, G. H. Gao, Y. Kuai and H. Zhang, *Soft Matter*, 2017, **13**, 1357–1363.
146. X. Cui, J. Li, Y. Hartanto, M. Durham, J. Tang, H. Zhang, G. Hooper, K. Lim and T. Woodfield, *Adv. Healthcare Mater.*, 2020, **9**, e1901648.

147. S. Ji and M. Guvendiren, *Front. Bioeng. Biotechnol.*, 2017, **5**, 23.
148. M. Kesti, C. Eberhardt, G. Pagliccia, D. Kenkel, D. Grande, A. Boss and M. Zenobi-Wong, *Adv. Funct. Mater.*, 2015, **25**, 7406–7417.
149. W. Dai, M. Sun, X. Leng, X. Hu and Y. Ao, *Front. Bioeng. Biotechnol.*, 2020, **8**, 604814.
150. D. Kilian, T. Ahlfeld, A. R. Akkineni, A. Bernhardt, M. Gelinsky and A. Lode, *Sci. Rep.*, 2020, **10**, 8277.
151. S. Duin, K. Schütz, T. Ahlfeld, S. Lehmann, A. Lode, B. Ludwig and M. Gelinsky, *Adv. Healthcare Mater.*, 2019, **8**, e1801631.
152. D. Joung, V. Truong, C. C. Neitzke, S. Z. Guo, P. J. Walsh, J. R. Monat, F. Meng, S. H. Park, J. R. Dutton, A. M. Parr and M. C. McAlpine, *Adv. Funct. Mater.*, 2018, **28**, 1801850.
153. L. Ouyang, J. P. K. Armstrong, Q. Chen, Y. Lin and M. M. Stevens, *Adv. Funct. Mater.*, 2020, **30**, 1908349.
154. D. Kilian, T. Ahlfeld, A. R. Akkineni, A. Bernhardt, M. Gelinsky and A. Lode, *Sci. Rep.*, 2020, **10**, 8277.
155. X. Li, Q. Deng, T. Zhuang, Y. Lu, T. Liu, W. Zhao, B. Lin, Y. Luo and X. Zhang, *Bio-Des. Manuf.*, 2020, **3**, 361–372.
156. F. Xu, J. Celli, I. Rizvi, S. Moon, T. Hasan and U. Demirci, *Biotechnol. J.*, 2011, **6**, 204–212.
157. J. W. Warrick, W. L. Murphy and D. J. Beebe, *IEEE Rev. Biomed. Eng.*, 2008, **1**, 75–93.
158. X. Wang, X. Li, X. Dai, X. Zhang, J. Zhang, T. Xu and Q. Lan, *Colloids Surf., B*, 2018, **171**, 291–299.
159. W. Zhu, B. Holmes, R. I. Glazer and L. G. Zhang, *Nanomedicine*, 2016, **12**, 69–79.
160. K. Chen, E. Jiang, X. Wei, Y. Xia, Z. Wu, Z. Gong, Z. Shang and S. Guo, *Lab Chip*, 2021, **21**, 1604–1612.
161. M. Duchamp, T. Liu, A. M. van Genderen, V. Kappings, R. Oklu, L. W. Ellisen and Y. S. Zhang, *Biotechnol. J.*, 2019, **14**, e1700703.
162. F. Bojin, A. Robu, M. I. Bejenariu, V. Ordodi, E. Olteanu, A. Cean, R. Popescu, M. Neagu, O. Gavriliuc, A. Neagu, S. Arjoca and V. Păunescu, *Micromachines*, 2021, **12**, 535.
163. R. H. Utama, L. Atapattu, A. P. O'Mahony, C. M. Fife, J. Baek, T. Allard, K. J. O'Mahony, J. C. C. Ribeiro, K. Gaus, M. Kavallaris and J. J. Gooding, *iScience*, 2020, **23**, 101621.
164. S. Swaminathan and A. M. Clyne, *J. Visualized Exp.*, 2020, **165**, e61791.
165. H. Horder, M. Guaza Lasheras, N. Grummel, A. Nadernezhad, J. Herbig, S. Ergün, J. Teßmar, J. Groll, B. Fabry, P. Bauer-Kreisel and T. Blunk, *Cells*, 2021, **10**, 803.
166. J. H. Li, C. T. Wu, P. K. Chu and M. Gelinsky, *Mater. Sci. Eng., R*, 2020, **140**, 100543.
167. J. Y. Park, H. Ryu, B. Lee, D.-H. Ha, M. Ahn, S. Kim, J. Y. Kim, N. L. Jeon and D.-W. Cho, *Biofabrication*, 2018, **11**, 015002.
168. S. B. Park, B. Koh, W. H. Jung, K. J. Choi, Y. J. Na, H. M. Yoo, S. Lee, D. Kang, D. M. Lee and K. Y. Kim, *Diabetes, Obes. Metab.*, 2020, **22**, 1302–1315.

169. H. Lee, J. Kim, Y. Choi and D. W. Cho, *ACS Biomater. Sci. Eng.*, 2020, **6**, 2469–2477.
170. Y. Zhao, R. Yao, L. Ouyang, H. Ding, T. Zhang, K. Zhang, S. Cheng and W. Sun, *Biofabrication*, 2014, **6**, 035001.
171. N. K. Singh, W. Han, S. A. Nam, J. W. Kim, J. Y. Kim, Y. K. Kim and D.-W. Cho, *Biomaterials*, 2020, **232**, 119734.
172. A. Srivastava, I. L. Isa, P. Rooney and A. Pandit, *Biomaterials*, 2017, **123**, 127–141.
173. T. A. Dixon, E. Cohen, D. M. Cairns, M. Rodriguez, J. Mathews, R. R. Jose and D. L. Kaplan, *Tissue Eng., Part C*, 2018, **24**, 346–359.
174. S. Das, S.-W. Kim, Y.-J. Choi, S. Lee, S.-H. Lee, J.-S. Kong, H.-J. Park, D.-W. Cho and J. Jang, *Acta Biomater.*, 2019, **95**, 188–200.
175. H. Lin, J. Tan, J. Zhu, S. Lin, Y. Zhao, W. Yu, H. Hojaiji, B. Wang, S. Yang, X. Cheng, Z. Wang, E. Tang, C. Yeung and S. Emaminejad, *Nat. Commun.*, 2020, **11**, 4405.
176. R. Gotor, P. Ashokkumar, M. Hecht, K. Keil and K. Rurack, *Anal. Chem.*, 2017, **89**, 8437–8444.
177. A. C. Da Silva, J. Wang and I. R. Minev, *Nat. Commun.*, 2022, **13**, 1353.
178. T. Distler and A. R. Boccaccini, *Acta Biomater.*, 2020, **101**, 1–13.
179. J. Xu, Y.-L. Tsai and S.-H. Hsu, *Molecules*, 2020, **25**, 5296.
180. D. Bruen, C. Delaney, J. Chung, K. Ruberu, G. G. Wallace, D. Diamond and L. Florea, *Macromol. Rapid Commun.*, 2020, **41**, e1900610.
181. D. Jiang, K. Sheng, H. Jiang and L. Wang, *Bioelectrochemistry*, 2021, **142**, 107919.
182. A. V. Bayles, T. Pleij, M. Hofmann, F. Hauf, T. Tervoort and J. Vermant, *ACS Appl. Mater. Interfaces*, 2022, **14**, 15667–15677.
183. G. Zidan, C. A. Greene, A. Etxabide, I. D. Rupenthal and A. Seyfoddin, *Int. J. Pharm.*, 2021, **599**, 120452.
184. S. Liu and L. Li, *ACS Appl. Mater. Interfaces*, 2017, **9**, 26429–26437.
185. J. Wang, Y. Liu, S. Su, J. Wei, S. E. Rahman, F. Ning, G. Christopher, W. Cong and J. Qiu, *Polymers*, 2019, **11**, 1873.
186. Z. Zhu, H. S. Park and M. C. McAlpine, *Sci. Adv.*, 2020, **6**, eaba5575.
187. S. E. Bakarich, R. Gorkin, M. I. H. Panhuis and G. M. Spinks, *Macromol. Rapid Commun.*, 2015, **36**, 1211–1217.
188. A. S. Gladman, E. A. Matsumoto, R. G. Nuzzo, L. Mahadevan and J. A. Lewis, *Nat. Mater.*, 2016, **15**, 413–418.
189. S. X. Wei, W. Lu, X. X. Le, C. X. Ma, H. Lin, B. Y. Wu, J. W. Zhang, P. Theato and T. Chen, *Angew. Chem., Int. Ed.*, 2019, **58**, 16243–16251.
190. K. Y. Lee, S.-J. Park, D. G. Matthews, S. L. Kim, C. A. Marquez, J. F. Zimmerman, H. A. M. Ardoña, A. G. Kleber, G. V. Lauder and K. K. Parker, *Science*, 2022, **375**, 639–647.
191. S. S. Ovunc, M. Yassin, R. Chae, A. Aba and R. Rodriguez Rubio, *Cureus*, 2021, **13**, e16749.

192. J. Li and M. Pumera, *Chem. Soc. Rev.*, 2021, **50**, 2794–2838.
193. W. Zhu, J. X. Li, Y. J. Leong, I. Rozen, X. Qu, R. F. Dong, Z. G. Wu, W. Gao, P. H. Chung, J. Wang and S. C. Chen, *Adv. Mater.*, 2015, **27**, 4411–4417.
194. J. Park, J. Y. Kim, S. Pané, B. J. Nelson and H. Choi, *Adv. Healthcare Mater.*, 2021, **10**, e2001096.
195. A. B. Baker, S. R. G. Bates, T. M. Llewellyn-Jones, L. P. B. Valori, M. P. M. Dicker and R. S. Trask, *Mater. Des.*, 2019, **163**, 107544.